Article

SOURCE DATA | TRANSPARENT PROCESS

THE EMBO JOURNAL

Cul3-Klhl18 ubiquitin ligase modulates rod transducin translocation during light-dark adaptation

Taro Chaya, Ryotaro Tsutsumi, Leah Rie Varner, Yamato Maeda, Satoyo Yoshida & Takahisa Furukawa*

Abstract

Adaptation is a general feature of sensory systems. In rod photoreceptors, light-dependent transducin translocation and Ca^{2+} homeostasis are involved in light/dark adaptation and prevention of cell damage by light. However, the underlying regulatory mechanisms remain unclear. Here, we identify mammalian Cul3-Klhl18 ubiquitin ligase as a transducin translocation modulator during light/dark adaptation. Under dark conditions, *Klhl18*$^{-/-}$ mice exhibited decreased rod light responses and subcellular localization of the transducin α-subunit (Tα), similar to that observed in light-adapted *Klhl18*$^{+/+}$ mice. Cul3-Klhl18 promoted ubiquitination and degradation of Unc119, a rod Tα-interacting protein. Unc119 overexpression phenocopied Tα mislocalization observed in *Klhl18*$^{-/-}$ mice. Klhl18 weakly recognized casein kinase-2-phosphorylated Unc119 protein, which is dephosphorylated by Ca^{2+}-dependent phosphatase calcineurin. Calcineurin inhibition increased Unc119 expression and Tα mislocalization in rods. These results suggest that Cul3-Klhl18 modulates rod Tα translocation during light/dark adaptation through Unc119 ubiquitination, which is affected by phosphorylation. Notably, inactivation of the Cul3-Klhl18 ligase and calcineurin inhibitors FK506 and cyclosporine A that are known immunosuppressant drugs repressed light-induced photoreceptor damage, suggesting potential therapeutic targets.

Keywords cilium; G protein; post-translational modification; protein transport; retina

Subject Categories Neuroscience; Post-translational Modifications & Proteolysis

DOI 10.15252/embj.2018101409 | Received 19 December 2018 | Revised 30 September 2019 | Accepted 8 October 2019 | Published online 7 November 2019

The EMBO Journal (2019) 38: e101409

Introduction

Vision in vertebrates begins with light reception and conversion to electrical signals through the process of phototransduction by rod and cone photoreceptor cells (Yau & Hardie, 2009). Rod photoreceptors are sensitive to a lower range of light intensities and are responsible for low light vision, while cone photoreceptors operate at brighter intensities and are responsible for high-resolution daylight and color vision. Paradoxically, light is also harmful to these photoreceptor cells. In some animal models of retinal degenerative diseases, including retinitis pigmentosa (RP) and Leber congenital amaurosis (LCA), photoreceptor degeneration is accelerated by light exposure and photoreceptors are protected by dark rearing (Paskowitz *et al*, 2006). In humans, exposure to light is a suspected risk factor for the progression of age-related macular degeneration (AMD) and RP (Parmeggiani *et al*, 2011; Marquioni-Ramella & Suburo, 2015; Schick *et al*, 2016; Mitchell *et al*, 2018).

Adaptation, a general phenomenon observed in sensory systems, makes it possible for sensory cells to respond to ambient signals appropriately according to background levels. Rod and cone photoreceptor cells alter their photosensitivity depending on ambient light levels, enabling responses to a wide range of light intensities (Fain *et al*, 2001; Luo *et al*, 2008). In darkness, rod photoreceptors become sensitive to light and ultimately can respond even to single photons (Baylor *et al*, 1979; Rieke & Baylor, 1998). On the other hand, they possess the ability to reduce light sensitivity and thus avoid excessive activation, preventing saturation and protecting them from brighter light (Fain, 2006). Since rod photoreceptor degeneration leads to secondary cone photoreceptor death, rod photoreceptor protection contributes to the preservation of vision under both dim light and daylight conditions (Roska & Sahel, 2018). Accordingly, light and dark adaptation of rod photoreceptors plays a crucial role in the acquisition of proper vision and in the prevention of blindness; however, the underlying regulatory mechanisms are not fully understood.

In rod photoreceptor cells, subcellular localization of transducin, a heterotrimeric G protein that is a component of the phototransduction cascade, changes in response to ambient light, thereby contributing to light and dark adaptation (Brann & Cohen, 1987; Philp *et al*, 1987; Whelan & McGinnis, 1988; Organisciak *et al*, 1991; Sokolov *et al*, 2002). Transducin is concentrated in the outer segment under dark-adapted conditions. After light reception, transducin is translocated from the outer segment to the inner part of the rod photoreceptor. This light- and dark-dependent transducin translocation is known to modulate photosensitivity in rod photoreceptors. For example, transgenic mice expressing a mutant form of the α-subunit of transducin (Tα), in which Tα acylation and localization to the outer segment are inhibited, show a

Laboratory for Molecular and Developmental Biology, Institute for Protein Research, Osaka University, Osaka, Japan
*Corresponding author. Tel: +81-6-6879-8631; Fax: +81-6-6879-8633; E-mail: takahisa.furukawa@protein.osaka-u.ac.jp

decreased light sensitivity of rod photoreceptors (Kerov *et al*, 2007). In contrast, mouse lines modeling Usher syndrome, *shaker1* and *whirler*, exhibit defective Tα translocation to the inner part and a decreased threshold of light-triggered photoreceptor degeneration (Peng *et al*, 2011; Tian *et al*, 2014). Furthermore, additional lipid modification by an amino acid substitution partially blocks light-induced Tα translocation from the outer segment to the inner part, leading to photoreceptor cell death (Kerov & Artemyev, 2011; Majumder *et al*, 2013).

In the current study, we identified the cullin 3 (Cul3)–Kelch-like 18 (Klhl18) ubiquitin E3 ligase as a modulator of transducin translocation during light and dark adaptation of rod photoreceptor cells. We found that *Klhl18* is predominantly expressed in retinal photoreceptor cells. Decreased light responses and Tα mislocalization from the outer segment to the inner part were observed in the rod photoreceptors of $Klhl18^{-/-}$ mice. Unc119, an interactor with Tα, is ubiquitinated and degraded by the Cul3–Klhl18 ligase. Overexpression of Unc119 phenocopied the Tα mislocalization observed in the $Klhl18^{-/-}$ retina. Unc119 expression in rod photoreceptors decreased under dark conditions in a Klhl18-dependent manner. Unc119 is phosphorylated and dephosphorylated by casein kinase 2 (CK2) and calcineurin, a Ca^{2+}-dependent phosphatase, respectively. Unc119 degradation by Cul3–Klhl18 is suppressed by Unc119 phosphorylation. Taken together, these results suggest that Cul3–Klhl18 modulates light- and dark-dependent Tα localization changes in rod photoreceptors through Unc119 ubiquitination and degradation, which is affected by Unc119 phosphorylation and dephosphorylation. Notably, genetic or pharmacological inactivation of the Cul3–Klhl18 ligase and calcineurin inhibitors FK506 and cyclosporine A (CsA) that are known immunosuppressant drugs repressed light-induced photoreceptor damage. Our results also suggest potential therapeutic targets for photoreceptor protection.

Results

Klhl18 is expressed in retinal photoreceptor cells

In order to identify molecules regulating retinal photoreceptor development and/or function, we searched for genes enriched in photoreceptor cells using our previously generated microarray data comparing transcripts between control and *Otx2* conditional knockout retinas, in which cell fate is converted from photoreceptors to amacrine-like cells (Nishida *et al*, 2003; Omori *et al*, 2011). We focused on *Klhl18*, which encodes a Cul3 ubiquitin E3 ligase substrate adaptor whose *in vivo* function has not yet been reported (Moghe *et al*, 2012). To examine the tissue distribution of *Klhl18* expression, we performed RT–PCR analysis using 4-week-old (4 weeks) mouse tissues. We observed *Klhl18* expression in the retina but not in other tissues examined (Fig 1A). We next carried out *in situ* hybridization analysis using developing and mature mouse retinal sections. We observed that *Klhl18* is expressed in the outer nuclear layer (ONL), where photoreceptor cells are located, at postnatal day 9 (P9) and P21 (Fig 1B, Appendix Fig S1). These results suggest that *Klhl18* is predominantly expressed in maturing and mature retinal photoreceptor cells.

Klhl18 deficiency decreases light response in rod photoreceptor cells

To investigate roles of the Cul3–Klhl18 ligase in retinal photoreceptor development and/or function, we generated *Klhl18* flox mice by targeted gene disruption (Fig EV1A). We mated the *Klhl18* flox mice with *CAG-Cre* mice, in which Cre recombinase is expressed in female germ cells (Sakai & Miyazaki, 1997), and generated conventional *Klhl18*-deficient ($Klhl18^{-/-}$) mice (Fig EV1A and B). In the $Klhl18^{-/-}$ retina, no Klhl18 mRNA or protein expression was detected by RT–PCR and Western blot with an anti-Klhl18 antibody that we generated (Fig EV1C and D). We observed substantial Klhl18 immunofluorescence signals in the inner segment (IS) and ONL in the $Klhl18^{+/+}$ retina but not in the $Klhl18^{-/-}$ retina (Fig EV1E). $Klhl18^{-/-}$ mice were viable and fertile, and exhibited no gross morphological abnormalities.

To examine the electrophysiological properties of the $Klhl18^{-/-}$ retina, we measured the electroretinograms (ERGs) of $Klhl18^{-/-}$ mice under dark-adapted (scotopic) and light-adapted (photopic) conditions. Under scotopic conditions, the amplitude of a-waves and b-waves, originating mainly from the population activity of rod photoreceptor cells (a-waves) and of rod bipolar cells (b-waves), significantly decreased in $Klhl18^{-/-}$ mice compared with that of $Klhl18^{+/+}$ mice (Fig 1C–E). To evaluate synaptic transmission from rod photoreceptors to rod bipolar cells, we calculated the scotopic b/a-wave ratio. We did not observe a significant difference in the scotopic b/a-wave ratio between $Klhl18^{+/+}$ and $Klhl18^{-/-}$ mice (Fig EV1F). In contrast, under photopic conditions, the amplitude of a-waves and b-waves, mainly reflecting the population activity of cone photoreceptor cells (a-waves) and of cone ON bipolar cells (b-waves), was comparable between $Klhl18^{+/+}$ and $Klhl18^{-/-}$ mice (Fig 1F–H). These results suggest that rod photoreceptor function is compromised by *Klhl18* deficiency, but not cone photoreceptor function.

To investigate how the scotopic ERG amplitude decreased in $Klhl18^{-/-}$ mice, we performed histological analyses using retinal sections. Toluidine blue staining showed that the ONL thickness was comparable between $Klhl18^{+/+}$ and $Klhl18^{-/-}$ retinas (Fig 2A and B). Immunohistochemical examination using marker antibodies against rhodopsin (rod outer segments), Rom1 (rod outer segments), S-opsin (S-cone outer segments), and M-opsin (M-cone outer segments) showed no substantial differences between $Klhl18^{+/+}$ and $Klhl18^{-/-}$ rod and cone outer segments (Fig EV2A–C). We also performed immunohistochemical analysis using antibodies against Chx10 (a marker for bipolar cells), Pax6 (a marker for amacrine and ganglion cells), calbindin (a marker for horizontal cells and a part of amacrine cells), Brn3a (a marker for ganglion cells), and S100β (a marker for Müller glial cells) and found no substantial differences between the $Klhl18^{+/+}$ and $Klhl18^{-/-}$ retinas (Fig EV2D–G). To observe whether photoreceptor degeneration occurs in the $Klhl18^{-/-}$ retina, we measured the ONL thickness in the $Klhl18^{-/-}$ retina at 6 months. No significant change was observed in the ONL thickness between $Klhl18^{+/+}$ and $Klhl18^{-/-}$ retinas (Fig EV2H and I).

Inhibition of the Cul3–Klhl18 ligase activity causes mislocalization of rod Tα

It was previously reported that mice having a substitution of aspartic acid for glycine at residue 90 of mouse Rhodopsin, a G

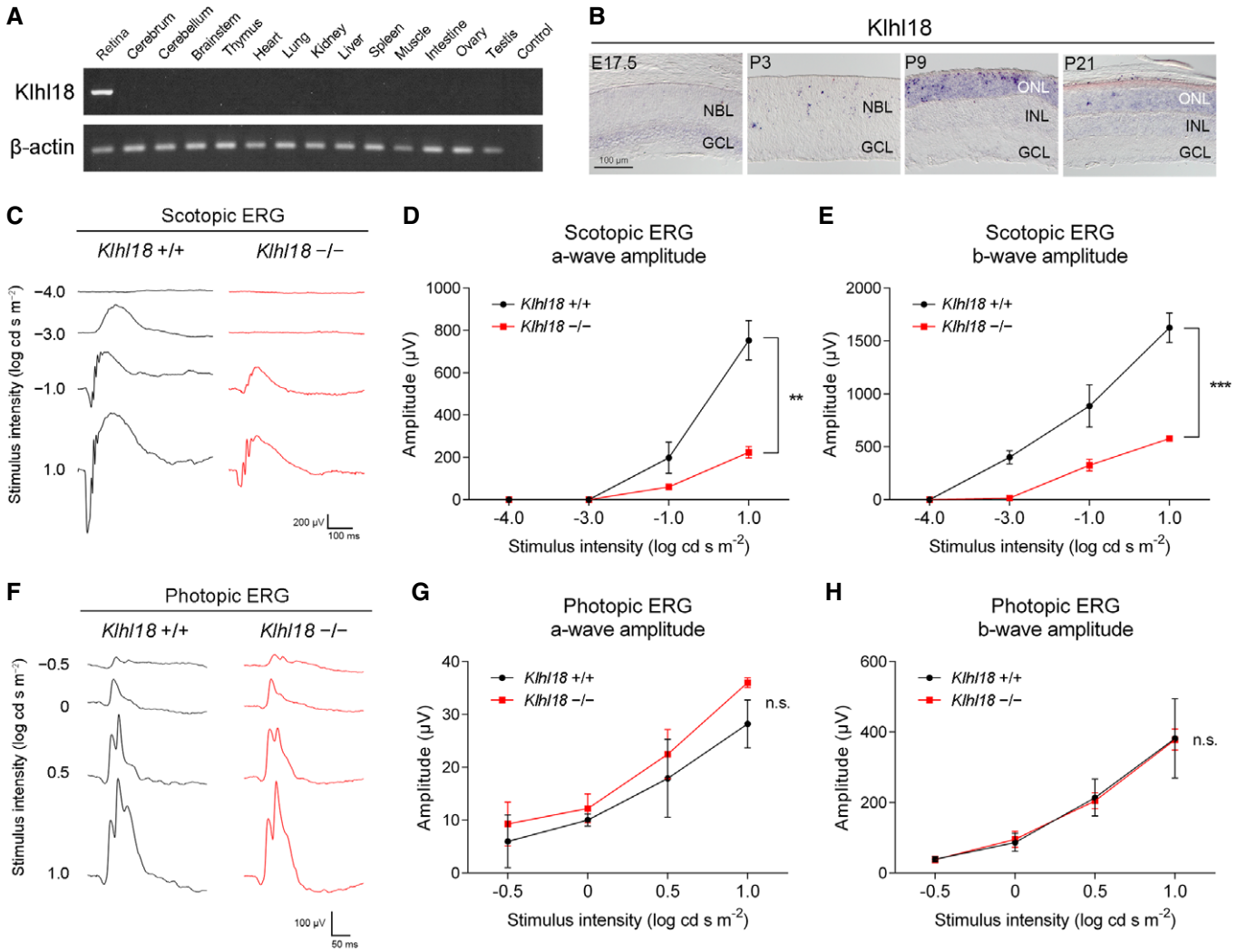

Figure 1. Decrease in the rod light responses in *Klhl18*$^{-/-}$ mice.

A RT–PCR analysis of the *Klhl18* transcript in mouse tissues at 4 weeks. *Klhl18* was predominantly expressed in the retina. *β-Actin* was used as a loading control.

B *In situ* hybridization analysis of *Klhl18* in developing (embryonic day 17.5 (E17.5), P3, and P9) and mature (P21) mouse retinas. *Klhl18* signals were detected in the ONL at P9 and P21. GCL, ganglion cell layer; NBL, neuroblastic layer; ONL, outer nuclear layer; INL, inner nuclear layer

C–H ERG analysis of *Klhl18*$^{-/-}$ mice. ERGs were recorded from *Klhl18*$^{+/+}$ and *Klhl18*$^{-/-}$ mice at 1 month (1 M) (n = 3 per each genotype). (C) Representative scotopic ERGs elicited by four different stimulus intensities (−4.0 to 1.0 log cd s/m^2) from *Klhl18*$^{+/+}$ and *Klhl18*$^{-/-}$ mice are presented. (D, E) The scotopic amplitudes of a- (D) and b-waves (E) are shown as a function of the stimulus intensity. Data are presented as mean ± SD. n = 3 per each genotype. $^{**}P < 0.01$, $^{***}P < 0.001$ (two-way repeated-measures ANOVA). (F) Representative photopic ERGs elicited by four different stimulus intensities (−0.5 to 1.0 log cd s/m^2) from *Klhl18*$^{+/+}$ and *Klhl18*$^{-/-}$ mice are presented. (G, H) The photopic amplitudes of a- (G) and b-waves (H) are shown as a function of the stimulus intensity. Data are presented as mean ± SD. n = 3 per each genotype. n.s., not significant (two-way repeated-measures ANOVA).

protein-coupled receptor, show constitutive light adaptation of rod photoreceptor cells (Sieving *et al*, 2001). These mice exhibit decreased rod light sensitivity without any changes in rod photoreceptor cell number and outer segment formation, resembling *Klhl18*$^{-/-}$ mice. Thus, we hypothesized that *Klhl18*$^{-/-}$ mice present constitutive light adaptation of rod photoreceptors and then observed the subcellular distribution of transducin in rod photoreceptor cells, which depends on ambient light conditions (Calvert *et al*, 2006). In the *Klhl18*$^{+/+}$ retina, rod Tα was localized mainly in the outer segment in the dark-adapted state, whereas Tα was translocated to the inner part of the photoreceptors in the light-adapted state. Contrastingly, in the *Klhl18*$^{-/-}$ retina, we found increased Tα localization to the inner part of photoreceptors in the dark-adapted state, as observed in light-adapted *Klhl18*$^{+/+}$ mice. In the light-adapted state, we also observed increased Tα localization to the inner part of photoreceptors in the *Klhl18*$^{-/-}$ retina compared with that in the *Klhl18*$^{+/+}$ retina (Fig 2C and D). On the other hand, we did not find significant differences in the transducin γ-subunit (Tγ) localization in the inner part of photoreceptors between *Klhl18*$^{+/+}$ and *Klhl18*$^{-/-}$ retinas under dark or light conditions

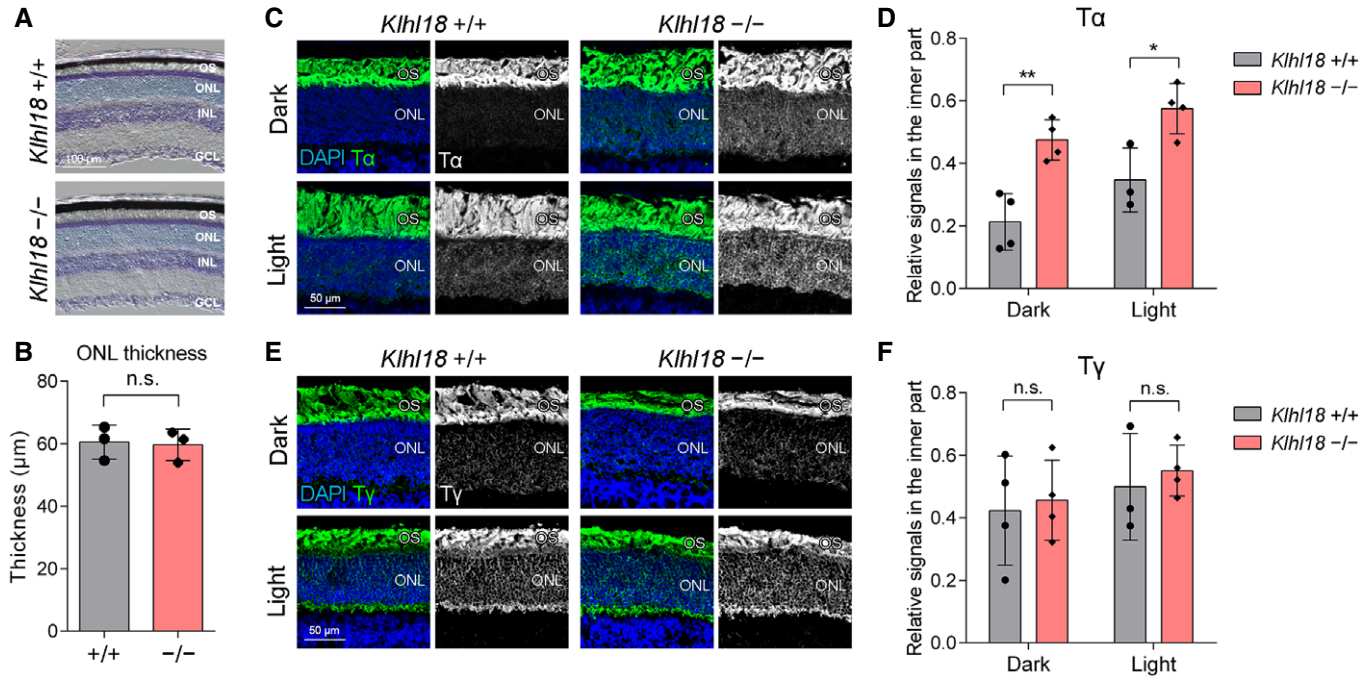

Figure 2. Rod Tα mislocalization in the *Klhl18*$^{-/-}$ mouse retina.

A, B Toluidine blue staining of retinas from *Klhl18*$^{+/+}$ and *Klhl18*$^{-/-}$ mice at 1 M. The ONL thickness was measured. Data are presented as mean ± SD. n.s., not significant (unpaired *t*-test), $n = 3$ mice per genotype.

C–F Subcellular localization of Tα and Tγ in photoreceptor cells of the *Klhl18*$^{-/-}$ retina. Retinal sections obtained from dark- or light- (~ 1,000 lx) adapted (4 h) *Klhl18*$^{+/+}$ and *Klhl18*$^{-/-}$ mice at 1 M were immunostained with an anti-Tα (C) or anti-Tγ (E) antibody. The immunofluorescence signals of Tα (D) and Tγ (F) detected in the inner part of photoreceptors were quantified using ImageJ software. The measured signals of Tα or Tγ in the inner part of photoreceptors were expressed as a proportion of the total (OS + the inner part) signals of Tα or Tγ in photoreceptors, respectively. Data are presented as mean ± SD. $n = 4, 4, 3$, and 4 mice (*Klhl18*$^{+/+}$; dark, *Klhl18*$^{-/-}$; dark, *Klhl18*$^{+/+}$; light, and *Klhl18*$^{-/-}$; light, respectively). *$P < 0.05$, **$P < 0.01$, n.s., not significant (unpaired *t*-test).

Data information: GCL, ganglion cell layer; ONL, outer nuclear layer; INL, inner nuclear layer; OS, outer segment.

(Fig 2E and F). In rod photoreceptors, the subcellular distribution of visual arrestin also changes in response to ambient light. After light reception, visual arrestin translocates from the inner part to the outer segment (Broekhuyse *et al*, 1985; Philp *et al*, 1987; Whelan & McGinnis, 1988). To investigate the subcellular localization of visual arrestin in *Klhl18*$^{+/+}$ and *Klhl18*$^{-/-}$ retinas under dark- and light-adapted conditions, we performed immunohistochemical analysis. While we observed light-triggered translocation of visual arrestin to the outer segment of rod photoreceptors, we did not find significant differences in the localization of visual arrestin in the inner part of photoreceptors between *Klhl18*$^{+/+}$ and *Klhl18*$^{-/-}$ retinas under dark- and light-adapted conditions (Fig EV2J and K).

To further investigate the role of Cul3–Klhl18 in subcellular localization of transducin in rod photoreceptor cells, we injected MLN4924, a small molecule inhibitor of the NEDD8-activating enzyme (NAE), into wild-type mice (Soucy *et al*, 2009). Covalent attachment of the ubiquitin-like protein Nedd8 to cullin family proteins is required for the function of the cullin-based ubiquitin E3 ligases (Pan *et al*, 2004). We observed increased Tα localization in the inner part of photoreceptors in the retina of MLN4924-treated mice compared with that of DMSO-treated mice under dark conditions (Fig EV3A and B). In contrast to Tα, Tγ localization to the inner part of retinal photoreceptors was not increased in MLN4924-treated mice (Fig EV3A and B). These results suggest that Cul3–Klhl18 is involved in the regulation of dark- and light-dependent Tα but not Tγ translocation in rod photoreceptor cells.

Light-induced retinal damage is suppressed by inhibiting the Cul3–Klhl18 ligase activity

It was previously reported that fixation of Tα to the outer segment increases light-triggered photoreceptor cell death (Majumder *et al*, 2013), suggesting that Tα translocation to the inner part decreases photoreceptor damage caused by light. To examine whether inhibition of Cul3–Klhl18 suppresses photoreceptor damage by light, *Klhl18*$^{+/+}$ and *Klhl18*$^{-/-}$ mice were exposed to light-emitting diode (LED) light and their retinal damage was compared (Fig 3A). We observed decreased ONL thickness in the *Klhl18*$^{+/+}$ retina compared with that in the *Klhl18*$^{-/-}$ retina (Fig 3B). To analyze light-induced retinal damage in more detail, we immunostained retinal sections using antibodies against Rhodopsin, S-opsin, M-opsin, and IbaI (a marker for macrophage and microglia). We observed that rod and cone outer segments were disorganized in the *Klhl18*$^{+/+}$ retina compared with those in the *Klhl18*$^{-/-}$ retina. The number of macrophages and/or microglia in the ONL increased in the *Klhl18*$^{+/+}$ retina compared with those in the *Klhl18*$^{-/-}$ retina (Figs 3C and EV3C). We also performed an ERG analysis and found that scotopic and photopic b-wave amplitudes in *Klhl18*$^{-/-}$ mice are higher than

those in *Klhl18*$^{+/+}$ mice, although no significant differences in scotopic and photopic a-wave amplitudes were detected between *Klhl18*$^{+/+}$ and *Klhl18*$^{-/-}$ mice (Figs 3D and E, and EV3D and E). The scotopic a-wave amplitude was significantly higher in *Klhl18*$^{+/+}$ mice compared with that in *Klhl18*$^{-/-}$ mice (Fig 1C and D), and this result shows that LED light exposure decreased the scotopic a-wave amplitude in *Klhl18*$^{+/+}$ mice more than in *Klhl18*$^{-/-}$ mice, suggesting that light-induced photoreceptor damage is suppressed in *Klhl18*$^{-/-}$ mice compared with that in *Klhl18*$^{+/+}$ mice.

We next exposed wild-type mice treated with DMSO or MLN4924 to LED light (Fig 3F). We observed a reduction in the ONL thickness in DMSO-treated mice compared with that in MLN4924-treated mice (Fig 3G). Immunohistochemical analysis showed more severely disorganized rod and cone outer segments and an increased number of macrophages and/or microglia localized to the ONL in DMSO-treated mice compared with those in MLN4924-treated mice (Figs 3H and EV3F). We also observed that scotopic and photopic b-wave amplitudes as well as scotopic a-wave amplitudes in MLN4924-treated mice are higher than those in DMSO-treated mice, although there were no significant differences in photopic a-wave amplitudes between DMSO- and MLN4924-treated mice (Figs 3I and J, and EV3G and H). Although we cannot deny the possibility that MLN4924 affects proteins other than Cul3–Klhl18 that require the NEDD8-activating enzyme, the results obtained using LED light-exposed *Klhl18*$^{-/-}$ mice and MLN4924-treated mice suggest that blocking Cul3–Klhl18 activity suppresses light-induced retinal damage.

Unc119 is a substrate for the Cul3–Klhl18 ligase

In light of Tα mislocalization in the retina of *Klhl18*$^{-/-}$ and MLN4924-treated mice, we focused on Unc119 as a candidate target for Cul3–Klhl18. It was previously reported that Unc119 is a lipid-binding protein interacting with the acylated N termini of Tα and that Unc119 suppresses rhodopsin-mediated transducin activation and dopamine D2 receptor-mediated G protein activation (Gopalakrishna *et al*, 2011; Zhang *et al*, 2011). Deletion of *Unc119* blocks the dark-triggered movement of Tα to the outer segment (Zhang *et al*, 2011). To test the interaction between Klhl18 and Unc119, we performed an immunoprecipitation assay using HEK293T cells with an anti-FLAG antibody and observed that Klhl18 is co-immunoprecipitated with Unc119 (Fig 4A and B). We also observed the interaction of *Caenorhabditis elegans* (*C. elegans*) kel-3, a homolog of mammalian Klhl18, with unc-119 by immunoprecipitation (Fig 4C). To further analyze the interaction between Klhl18 and Unc119, we carried out a GST pull-down assay using purified GST-fused human KLHL18 and polyhistidine (6xHis)-tagged human UNC119 and found a direct interaction between Klhl18 and Unc119 (Fig 4D and Appendix Fig S2A–C). This result was confirmed by a homogeneous time-resolved fluorescence (HTRF) assay using the purified proteins (Fig 4E, and Appendix Fig S2B and C). The Klhl18 protein possesses an N-terminal BTB-BACK domain and six Kelch repeats at the C terminus (Fig 4F; Dhanoa *et al*, 2013). Kelch-like proteins bind to Cul3 and their substrates through the BTB-BACK domain and Kelch repeats, respectively (Genschik *et al*, 2013). To determine which region of Klhl18 interacts with Unc119, we prepared constructs encoding Klhl18 truncation mutants containing either the BTB-BACK domain (Klhl18-N) or the Kelch repeats (Klhl18-C) as well as the full-length Klhl18 (Klhl18-FL) (Fig 4F) and assessed the interaction by an immunoprecipitation assay. As expected, Unc119 interacted with Klhl18-FL and Klhl18-C but not Klhl18-N (Fig 4G). To examine whether Cul3–Klhl18 degrades Unc119, HEK293T cells were transfected with a plasmid expressing Klhl18-FL, Klhl18-N, or Klhl18-C together with an Unc119 expression plasmid. We observed that Unc119 expression decreased in the presence of Klhl18-FL but not Klhl18-N nor Klhl18-C (Fig 4H). We also found decreased Unc119 expression by Klhl18-FL in Neuro2a cells, which was inhibited by proteasome inhibitor MG132 (Fig 4I). Similarly, the treatment of Neuro2a cells with MLN4924 suppressed the reduction in Unc119 expression levels by Klhl18-FL (Fig 4J). To address whether Cul3–Klhl18 ubiquitinates Unc119, we transfected Klhl18 and HA-tagged Unc119 expression plasmids together with a 6xHis-tagged ubiquitin expression plasmid into Neuro2a cells and performed a Ni-NTA pull-down under denaturing conditions. We observed that Klhl18 promotes polyubiquitination of Unc119 (Fig 4K). Altogether, these data suggest that Cul3–Klhl18 ubiquitinates and degrades Unc119.

Unc119 is a target of the Cul3–Klhl18 ligase in the retina

To examine whether Unc119 is degraded by Cul3–Klhl18 in the retina, we first analyzed Unc119 protein expression levels in *Klhl18*$^{+/+}$ and *Klhl18*$^{-/-}$ retinas. We raised an anti-Unc119 antibody that recognizes the Unc119 but not Unc119b protein by Western blot analysis (Fig EV4A). We immunostained retinal sections from *Klhl18*$^{+/+}$ and *Klhl18*$^{-/-}$ mice using an anti-Unc119 antibody and observed increased Unc119 signals in the photoreceptor layer of the *Klhl18*$^{-/-}$ retina compared with those of the *Klhl18*$^{+/+}$ retina (Fig 5A). To confirm this result, we also performed a Western blot analysis and found increased Unc119 protein expression in the *Klhl18*$^{-/-}$ retina compared with that of the *Klhl18*$^{+/+}$ retina (Fig 5B and C). We next examined Unc119 expression levels in the retina from DMSO- or MLN4924-injected mice by Western blotting, and found that MLN4924 treatment increases the Unc119 protein expression (Fig 5D and E). In contrast, there were no significant differences in *Unc119* mRNA expression levels between *Klhl18*$^{+/+}$ and *Klhl18*$^{-/-}$ retinas (Fig 5F). To further investigate whether Cul3–Klhl18 degrades Unc119 in the retina, we electroporated a plasmid encoding Klhl18-N into the retina *in vivo*. We observed an increase in Tα localization to the inner part of photoreceptors and increased Unc119 signal in the photoreceptor layer in the area where Klhl18-N is overexpressed, as shown by the GFP signal, under the dark-adapted condition (Fig EV4B and C). Together, these results suggest that Cul3–Klhl18 degrades Unc119 in the retina.

To investigate whether the rod Tα mislocalization observed in *Klhl18*$^{-/-}$ and MLN4924-treated mice is due to the increased expression of Unc119, we electroporated a plasmid encoding Unc119 into the retina *in vivo*. Consistent with *Klhl18*$^{-/-}$ and MLN4924-treated mice, we observed the increased Tα localization in the inner part of photoreceptors in the area where Unc119 is overexpressed as shown by GFP signals under dark conditions (Fig 5G and H). On the other hand, the subcellular distribution of Tγ was unchanged by Unc119 overexpression (Fig 5G and H). Collectively, these data suggest that Unc119 is a target of Cul3–Klhl18 in the retina.

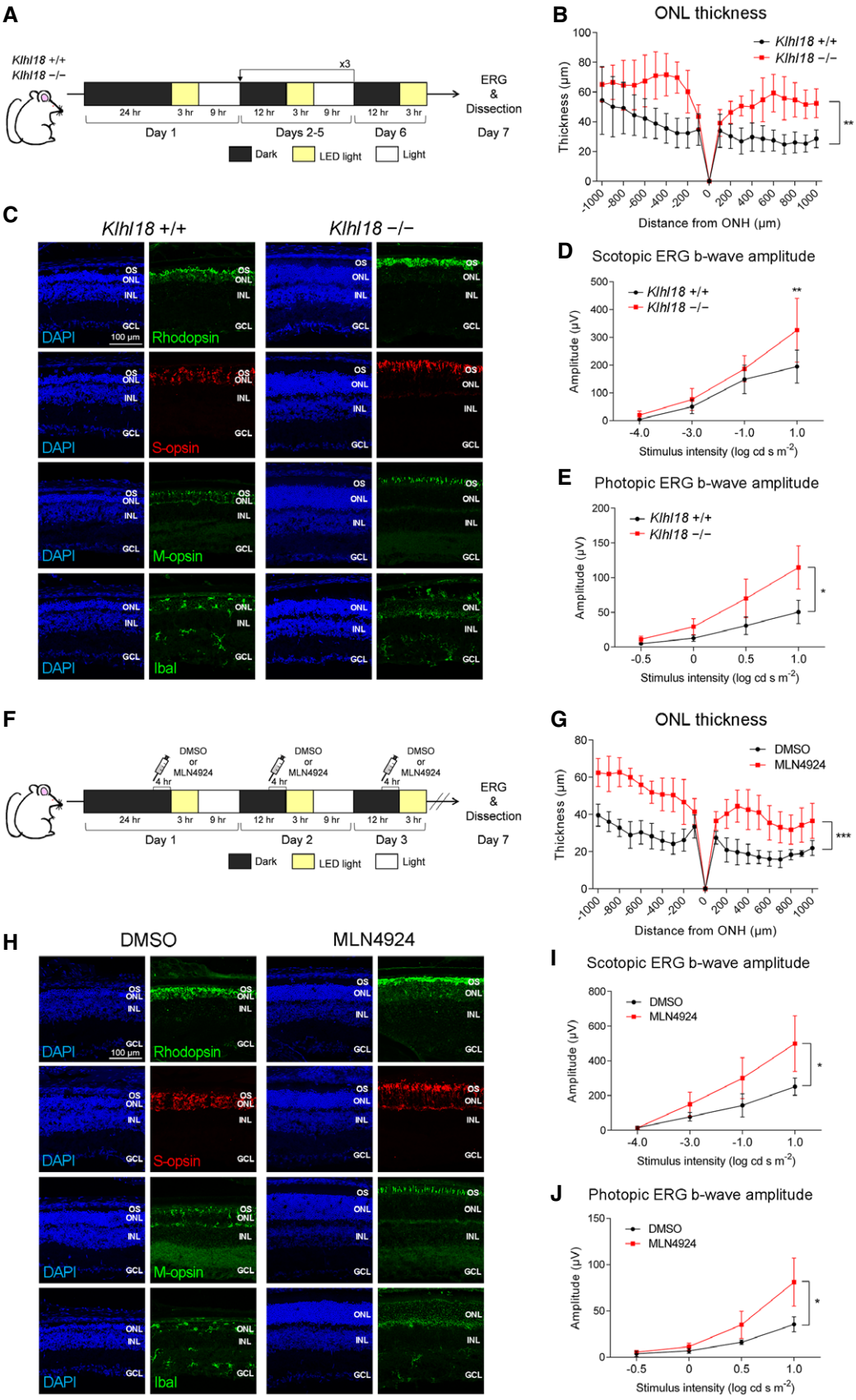

Figure 3.

Figure 3. Klhl18 deficiency represses light-induced retinal damage.

A Experimental design for exposure of *Klhl18*$^{+/+}$ and *Klhl18*$^{-/-}$ mice to LED light.

B Retinal sections from *Klhl18*$^{+/+}$ and *Klhl18*$^{-/-}$ mice after light exposure were stained with DAPI, and then, the ONL thickness was measured. Data are presented as mean ± SD. $^{**}P < 0.01$ (two-way repeated-measures ANOVA), $n = 5$ mice per genotype.

C Immunohistochemical analysis of retinas from *Klhl18*$^{+/+}$ and *Klhl18*$^{-/-}$ mice after light exposure using marker antibodies as follows: Rhodopsin (rod outer segments), S-opsin (S-cone outer segments), M-opsin (M-cone outer segments), and Iba1 (microglia or macrophages). Nuclei were stained with DAPI. Rod and cone outer segments were severely disorganized in the *Klhl18*$^{+/+}$ retina.

D, E ERG analysis of *Klhl18*$^{+/+}$ and *Klhl18*$^{-/-}$ mice after LED light exposure. Scotopic (D) and photopic (E) amplitudes of b-waves are shown as a function of the stimulus intensity. Data are presented as mean ± SD. $^{*}P < 0.05$ (two-way repeated-measures ANOVA), $^{**}P < 0.01$ (two-way repeated-measures ANOVA followed by Sidak's multiple comparisons test), $n = 4$ and 5 mice (*Klhl18*$^{+/+}$ and *Klhl18*$^{-/-}$, respectively).

F Experimental design for exposure of mice treated with MLN4924, an NAE inhibitor, to LED light. MLN4924 was injected into mice every day for 3 days.

G Retinal sections from MLN4924-treated mice after light exposure were stained with DAPI, and the ONL thickness was measured. Data are presented as mean ± SD. $^{***}P < 0.001$ (two-way repeated-measures ANOVA), $n = 4$ mice each.

H Immunohistochemical analysis of retinas from MLN4924-treated mice after light exposure using marker antibodies as follows: Rhodopsin (rod outer segments), S-opsin (S-cone outer segments), M-opsin (M-cone outer segments), and Iba1 (microglia or macrophages). Nuclei were stained with DAPI. Rod and cone outer segments were severely disorganized in the DMSO-injected retina.

I, J ERG analysis of MLN4924-treated mice after LED light exposure. The scotopic (I) and photopic (J) amplitudes of b-waves are shown as a function of the stimulus intensity. Data are presented as mean ± SD. $^{*}P < 0.05$, (two-way repeated-measures ANOVA), $n = 4$ mice each.

Data information; OS, outer segment; ONL, outer nuclear layer; INL, inner nuclear layer; GCL, ganglion cell layer. ONH, optic nerve head.

Unc119 is phosphorylated and dephosphorylated by CK2 and calcineurin, respectively

To investigate the conditions in which Unc119 is degraded by Cul3–Klhl18, we examined Unc119 protein expression in *Klhl18*$^{+/+}$ and *Klhl18*$^{-/-}$ retinas under dark and light conditions. In the *Klhl18*$^{+/+}$ retinas, Unc119 immunofluorescence signals in the photoreceptor layer were higher under light conditions than those under dark conditions (Fig 6A). In contrast, although Unc119 signals increased in the retina as a consequence of *Klhl18* deficiency as observed above (Fig 5A), no substantial differences in Unc119 signals were detected between dark and light conditions in the *Klhl18*$^{-/-}$ retinas (Fig 6A). Consistent with the immunofluorescence result, we found increased Unc119 protein expression under light conditions compared with that under dark conditions in the *Klhl18*$^{+/+}$ retina but not in the *Klhl18*$^{-/-}$ retina by Western blot analysis (Fig 6B and C). Light-induced Tα translocation to the inner part takes less time than Tα translocation to the outer segment under dark-adapted conditions. Within ~ 30 min after illumination, rod Tα translocates from the outer segment to the inner part (Sokolov *et al*, 2002; Rosenzweig *et al*, 2007; Slepak & Hurley, 2008). To examine whether Unc119 protein expression increases within this time range, wild-type retinas were harvested 15 min after the onset of light exposure. We observed increased Unc119 protein expression under the condition of 15 min of light adaptation compared with that under the dark-adapted condition (Fig EV4D and E). These results suggest that Cul3–Klhl18 efficiently degrades Unc119 in the retina under dark conditions, and that there are some mechanisms that regulate Cul3–Klhl18-mediated Unc119 degradation.

To elucidate these mechanisms, we focused on phosphorylation of the Unc119 protein, since high-throughput phosphoproteomic analyses have shown that Unc119 is phosphorylated at residues 37, 39, and 41 (PhosphoSitePlus) (Hornbeck *et al*, 2015), which were also predicted to be phosphorylated by NetPhos 3.1 (Blom *et al*, 1999). All these residues are located in the consensus sequence pS/T-X-X-E/D for phosphorylation by CK2, which is a serine/threonine kinase expressed in retinal photoreceptor cells (Fig 6D; Trojan *et al*, 2008). To test Unc119 phosphorylation by CK2, we performed an *in vitro* kinase assay. Phos-tag SDS–PAGE showed band shifts of 6xHis-tagged UNC119 by CK2, indicating that Unc119 can be directly phosphorylated by CK2 (Fig 6E). We then generated a construct encoding the UNC119 protein harboring Ser-to-Ala mutations at residues of the predicted CK2 phosphorylation sites (UNC119-SA). We observed that wild-type UNC119 but not UNC119-SA is phosphorylated by CK2 using Phos-tag Western blot analysis (Fig EV5A, and Appendix Fig S2D and E). These results show that CK2 directly phosphorylates Unc119, predominantly at residues 37, 39, and/or 41. We also examined Unc119 phosphorylation in the retina under dark and light conditions. We observed that Unc119 is more phosphorylated under light conditions compared with dark conditions by Phos-tag Western blotting (Fig 6F and G).

To understand the regulation of light-dependent Unc119 phosphorylation, we paid attention to the phosphatase(s) that could dephosphorylate Unc119. Calcineurin is the only known Ca^{2+}- and calmodulin-dependent serine/threonine protein phosphatase (Klee *et al*, 1979, 1998). In rod photoreceptor cells, intracellular Ca^{2+} concentration under dark conditions is higher than that under light conditions (Woodruff *et al*, 2002). Calcineurin is a heterodimeric protein composed of a catalytic and a regulatory subunit. In mammals, there are three isoforms of the catalytic subunit, Ppp3ca, Ppp3cb, and Ppp3cc, and two isoforms of the regulatory subunit, Ppp3r1 and Ppp3r2. We identified *Ppp3cc* as a candidate gene that is expressed in photoreceptor cells using our microarray data (Omori *et al*, 2011). To confirm this, we carried out an *in situ* hybridization analysis using mouse retinal sections and observed that *Ppp3cc* is expressed in the ONL (Fig EV5B). Since photoreceptor cells in the *Pde6b*$^{rd1/rd1}$ retina are degenerated (Keeler, 1924), the expression levels of genes enriched in retinal photoreceptor cells are predicted to decrease in the *Pde6b*$^{rd1/rd1}$ retina compared with those in the *Pde6b*$^{+/+}$ retina. *Ppp3cc* mRNA expression decreased in the *Pde6b*$^{rd1/rd1}$ retina, suggesting that *Ppp3cc* is expressed in retinal photoreceptors (Fig EV5C). To examine the interaction between Unc119 and the catalytic subunits of calcineurin, we performed an immunoprecipitation assay using HEK293T cells with an anti-FLAG antibody and observed that Unc119 interacts with Ppp3ca, Ppp3cb, and Ppp3cc (Fig 6H). To test Unc119 dephosphorylation by calcineurin, we performed an *in vitro* phosphatase assay. Phos-tag SDS–PAGE showed suppression of CK2-mediated band shifts of 6xHis-tagged UNC119 by calcineurin, indicating that Unc119 can be directly dephosphorylated by calcineurin (Fig 6I, Appendix Fig S2D).

Phosphorylation of Unc119 downregulates its degradation mediated by Klhl18

To investigate physiological roles of Unc119 phosphorylation, we performed an HTRF assay using GST-fused KLHL18 and 6xHis-tagged UNC119 with or without pretreatment with CK2. We found that Unc119 phosphorylation by CK2 suppresses the direct interaction between KLHL18 and UNC119 (Fig 7A, and Appendix Fig S2B and C). To test effects of Unc119 phosphorylation on Klhl18-mediated degradation, we generated a construct encoding the

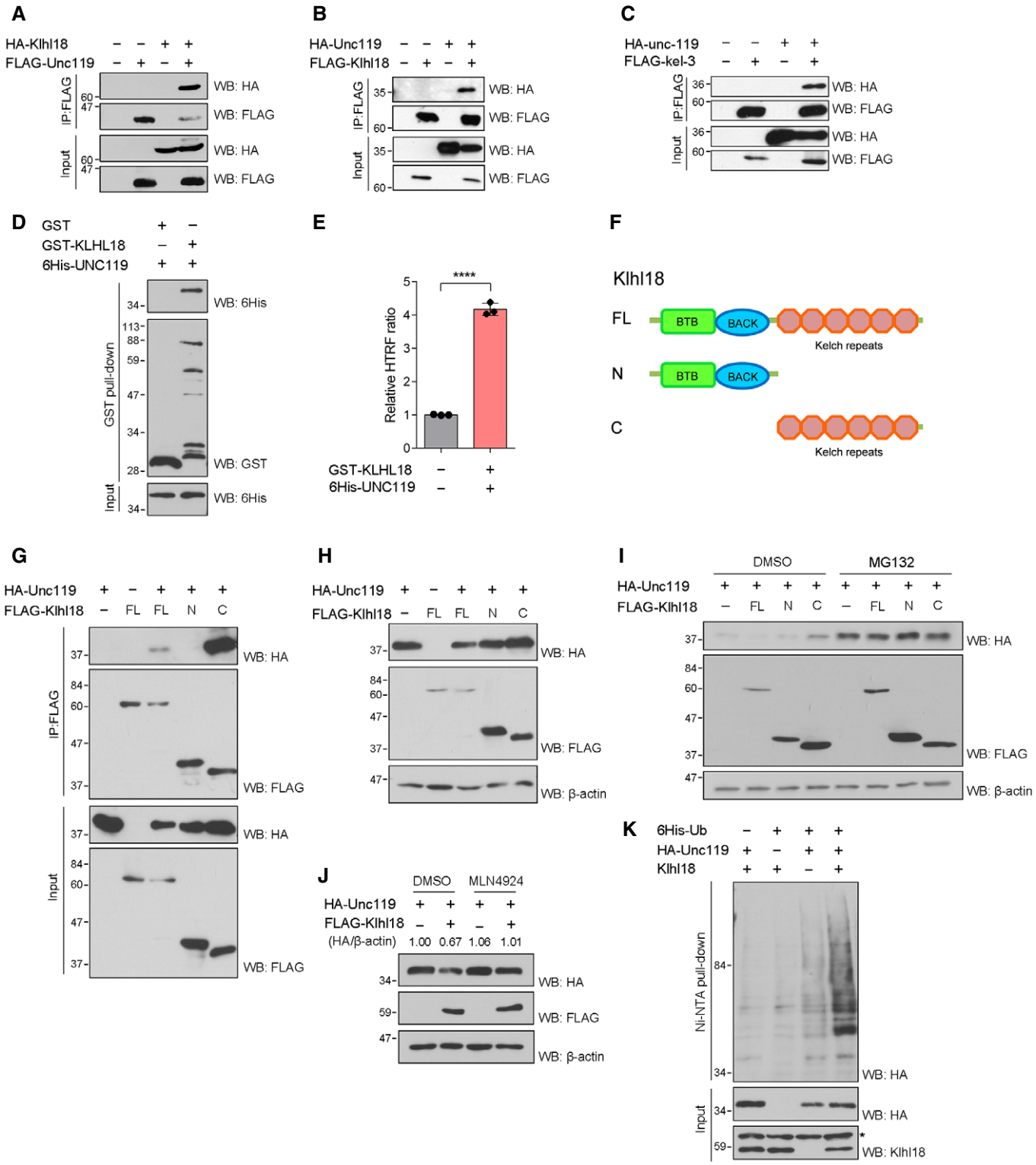

Figure 4.

Figure 4. Unc119 is a substrate of Cul3–Klhl18.

A, B Immunoprecipitation analysis of Klhl18 and Unc119. (A) HEK293T cells were transfected with plasmids expressing HA-tagged Klhl18 and FLAG-tagged Unc119. The cell lysates were subjected to immunoprecipitation with an anti-FLAG antibody. Immunoprecipitated proteins were analyzed by Western blotting with anti-FLAG and anti-HA antibodies. (B) HEK293T cells were transfected with plasmids expressing HA-tagged Unc119 and FLAG-tagged Klhl18. The cell lysates were subjected to immunoprecipitation with an anti-FLAG antibody. Immunoprecipitated proteins were analyzed by Western blotting with anti-FLAG and anti-HA antibodies.

C Immunoprecipitation analysis of *Caenorhabditis elegans* kel-3 and unc-119. HEK293T cells were transfected with plasmids expressing HA-tagged unc-119 and FLAG-tagged kel-3. The cell lysates were subjected to immunoprecipitation with an anti-FLAG antibody. Immunoprecipitated proteins were analyzed by Western blotting with anti-FLAG and anti-HA antibodies.

D, E *In vitro* binding of human KLHL18 to UNC119. (D) Recombinant GST or GST-fused human KLHL18 was incubated with recombinant 6xHis-tagged human UNC119. The mixtures were subjected to GST pull-down assay, and then, bound proteins were detected by Western blotting using an anti-6xHis antibody. (E) Recombinant GST-fused human KLHL18 and 6xHis-tagged human UNC119 proteins were incubated with anti-GST-d2 and anti-6HIS-Eu Gold antibodies. The mixtures were subjected to homogeneous time-resolved fluorescence (HTRF) assay, and then, the HTRF ratio was quantified. Data are presented as mean ± SD. ****$P < 0.0001$ (unpaired *t*-test), $n = 3$.

F Schematic diagrams of Klhl18 truncated mutants.

G Immunoprecipitation analysis of Klhl18 truncated mutants and Unc119. HEK293T cells were transfected with plasmids expressing HA-tagged Unc119 and the indicated FLAG-tagged Klhl18 mutants. The cell lysates were subjected to immunoprecipitation with an anti-FLAG antibody. Immunoprecipitated proteins were analyzed by Western blotting with anti-FLAG and anti-HA antibodies.

H Reduction in Unc119 expression in the presence of Klhl18. HEK293T cells were transfected with plasmids expressing HA-tagged Unc119 and the indicated FLAG-tagged Klhl18 constructs. The cell lysates were analyzed by Western blotting with anti-FLAG and anti-HA antibodies. β-Actin was used as a loading control.

I Proteasomal degradation of Unc119 by Klhl18. Neuro2a cells transfected with plasmids expressing HA-tagged Unc119 and the indicated FLAG-tagged Klhl18 mutants were treated with 10 μM MG132 or DMSO for 6 h before harvest. The cell lysates were analyzed by Western blotting with anti-HA and anti-FLAG antibodies. β-Actin was used as a loading control.

J Neuro2a cells transfected with plasmids expressing HA-tagged Unc119 and FLAG-tagged Klhl18 were treated with 0.3 μM MLN4924 or DMSO for 6 h before harvest. The cell lysates were analyzed by Western blotting with anti-HA and anti-FLAG antibodies. β-Actin was used as a loading control. Reduction in Unc119 expression by Klhl18 is inhibited by MLN4924.

K Unc119 ubiquitination by Klhl18. Neuro2a cells were transfected with plasmids expressing Klhl18, HA-tagged Unc119, and 6xHis-tagged ubiquitin. After 48 h, cells were lysed under denaturing conditions. Ubiquitinated proteins were pulled-down with Ni-NTA agarose beads, eluted, and analyzed by Western blotting with the anti-HA antibody. An asterisk indicates non-specific bands.

Source data are available online for this figure.

Unc119 protein harboring Ser-to-Ala mutations at residues 37, 39, and 41 (Unc119-SA). HEK293T cells were transfected with a plasmid encoding wild-type Unc119 or Unc119-SA together with a Klhl18 expression plasmid. We observed that Unc119-SA expression decreases in the presence of Klhl18 compared with Unc119-WT expression (Fig 7B and C). We next treated wild-type mice with CX4945, a small molecule inhibitor of CK2 (Siddiqui-Jain *et al*, 2010). Using Western blot analysis, we found that Unc119 expression in the retina decreased when treated with CX4945 (Fig 7D and E). In contrast, wild-type mice treated with FK506, a small molecule inhibitor of calcineurin (Liu *et al*, 1991), showed increased expression of Unc119 in the retina (Fig 7F and G). To investigate the role of calcineurin in the subcellular localization of transducin in rod photoreceptor cells, wild-type mice were injected with FK506. Consistent with increased Unc119 protein expression, mice treated with FK506 exhibited increased Tα localization to the inner part of photoreceptors compared with DMSO-treated mice under dark conditions (Fig 7H and I). In contrast, the Tγ localization in the inner part was unchanged between DMSO- and FK506-treated mice (Fig 7H and I). These results suggest that Unc119 phosphorylation downregulates Klhl18-mediated degradation.

Light-induced retinal damage is suppressed by inhibition of calcineurin activity

To address whether inhibition of calcineurin suppresses light-induced photoreceptor damage, mice treated with DMSO or FK506 were exposed to LED light and their retinal damage was compared (Fig 8A). We observed a reduced ONL thickness in DMSO-treated mice compared with that in FK506-treated mice (Fig 8B). To further analyze light-induced retinal damage, retinal sections were immunostained using antibodies against Rhodopsin, S-opsin, M-opsin, and IbaI. We found that rod and cone outer segments were disorganized in DMSO-treated mice compared with those in FK506-treated mice. We also observed an increased number of macrophages and/or microglia in the ONL of DMSO-injected mice compared with that of FK506-injected mice (Figs 8C and EV5D). To confirm this result, mice injected with another small molecule inhibitor of calcineurin, CsA, were exposed to LED light (Fig EV5E; Liu *et al*, 1991). We compared retinal damage between DMSO- and CsA-treated mice by histological analysis, and found decreased ONL thickness and more severely disorganized rod and cone outer segments in DMSO-treated mice compared with CsA-treated mice (Fig EV5F and G). Together, these results suggest that inhibition of calcineurin activity suppresses light-triggered photoreceptor damage in the retina.

Discussion

Based on the results of this study and previous reports, we propose a hypothetical model in which Cul3–Klhl18 promotes Unc119 ubiquitination and degradation through phosphorylation in a light- and dark-dependent manner, thereby modulating Tα translocation in rod photoreceptors (Fig EV5H). A previous report demonstrated that knockdown of either *Cul3* or *Klhl18* delays mitotic entry in cultured cells (Moghe *et al*, 2012). We observed that *Klhl18*$^{-/-}$ mice are viable and fertile without gross morphological abnormalities. In the *Klhl18*$^{-/-}$ retina, the ONL thickness and major cell composition were not different from those in the *Klhl18*$^{+/+}$ retina. Thus, defects in the cell cycle progression caused by loss of function of the Cul3–Klhl18 ligase might be compensated for *in vivo*. We also observed

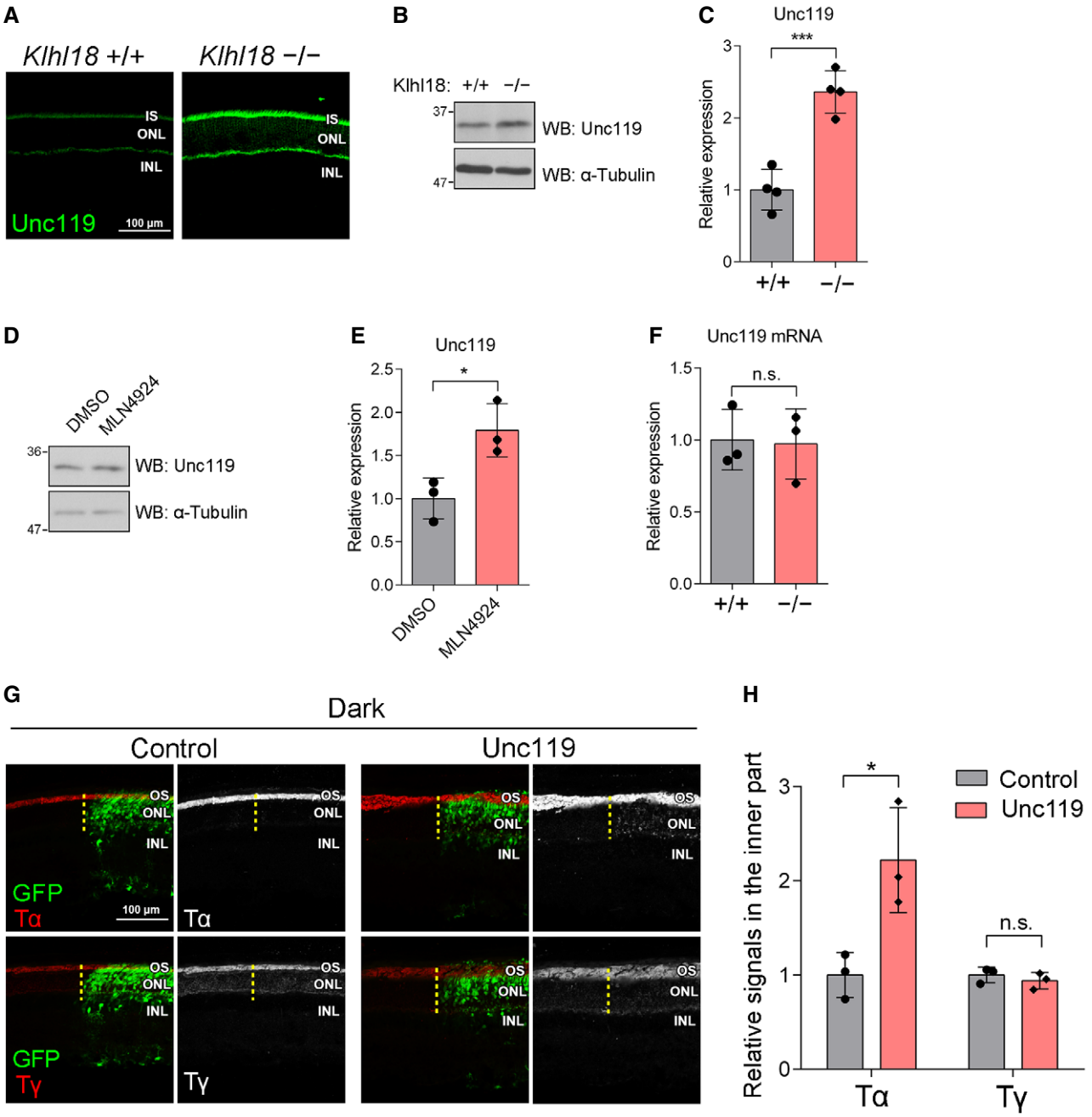

Figure 5.

no substantial differences between *Klhl18*$^{+/+}$ and *Klhl18*$^{-/-}$ rod outer segments by immunohistochemistry. In addition, no significant change was observed in the ONL thickness between *Klhl18*$^{+/+}$ and *Klhl18*$^{-/-}$ retinas at 6 months. Instead, *Klhl18*$^{-/-}$ mice exhibited a decreased response to light under dark-adapted conditions and rod Tα mislocalization.

It was previously reported that inhibition of Tα translocation to the outer segment reduces the rod light response (Kerov *et al*, 2007). This observation suggests that rod Tα mislocalization to the inner part resulting from *Klhl18* deficiency contributes to decreases in scotopic ERG amplitudes, although we cannot conclude that the observed mislocalization is the sole cause of decreases in the rod light response. We observed increased amounts of the Unc119 protein in *Klhl18*$^{-/-}$ rod photoreceptors. Unc119 overexpression caused increased Tα localization in the inner part of retinal photoreceptors. These observations suggest that Tα mislocalization observed in the *Klhl18*$^{-/-}$ retina is at least partially due to the increased amount of Unc119 protein. In addition to Tα, Unc119 interacts with other myristoylated proteins that are transported to cilia including the ciliopathy protein Nphp3 (Wright *et al*, 2011; Jean & Pilgrim, 2017), suggesting impaired trafficking of the myristoylated proteins to the outer segment in *Klhl18*$^{-/-}$ rod photoreceptors. On the other hand, Unc119 is localized to the photoreceptor ribbon synapse and proposed to be involved in synaptic vesicle

Figure 5. Unc119 is a target of Cul3–Klhl18 in the retina.

A Immunostaining of retinal sections from *Klhl18*$^{+/+}$ and *Klhl18*$^{-/-}$ mice with an anti-Unc119 antibody (green). The Unc119 signal in the IS, ONL, and INL increased in the *Klhl18*$^{-/-}$ retina.

B, C Western blot analysis of the Unc119 protein in *Klhl18*$^{+/+}$ and *Klhl18*$^{-/-}$ retinas. Unc119 expression increased in the *Klhl18*$^{-/-}$ retina. α-Tubulin was used as a loading control (B). Relative Unc119 protein levels in *Klhl18*$^{+/+}$ and *Klhl18*$^{-/-}$ retinas were determined by quantification of Unc119 band intensity (normalized to α-tubulin) (C). Data are presented as mean ± SD. ***$P < 0.001$ (unpaired *t*-test), $n = 4$ mice per genotype.

D, E Western blot analysis of the Unc119 protein in the retina from mice treated with DMSO or MLN4924 for 4 days. Wild-type mice were dark-adapted for 4 h before harvest. Unc119 expression increased in the retina from MLN4924-injected mice. α-Tubulin was used as a loading control (D). Relative Unc119 protein levels were determined by quantification of Unc119 band intensity (normalized to α-tubulin) (E). Data are presented as mean ± SD. *$P < 0.05$ (unpaired *t*-test), $n = 3$ mice each.

F Quantitative RT–PCR analysis of the *Unc119* mRNA in *Klhl18*$^{+/+}$ and *Klhl18*$^{-/-}$ retinas at 1 M. No significant difference was detected between *Klhl18*$^{+/+}$ and *Klhl18*$^{-/-}$ retinas. Data are presented as mean ± SD. n.s., not significant (unpaired *t*-test), $n = 3$ mice per genotype.

G, H Subcellular localization of Tα and Tγ in Unc119-overexpressing photoreceptor cells. (G) The pCIG (empty vector) or pCIG-Flag-Unc119 plasmid was electroporated into P0 mouse retinas. At 1 M, the mice were dark-adapted for 4 h, and then, their retinas were harvested, sectioned, and immunostained with anti-Tα and anti-Tγ antibodies. The electroporated cells express EGFP mediated by the IRES sequence. The Tα signal in the inner part of photoreceptors increased in the pCIG-Flag-Unc119-electroporated regions. Yellow broken lines indicate boundaries between the GFP-positive and GFP-negative regions. (H) The immunofluorescence signals of Tα and Tγ detected in the inner part of photoreceptors were quantified using ImageJ software. The signals of Tα or Tγ in the inner part of photoreceptors were normalized to the total (OS + the inner part) signals of Tα or Tγ in photoreceptors, respectively. Tα or Tγ signals in the inner part (normalized to the total signals) of GFP-positive regions relative to those of GFP-negative regions were then calculated. Data are presented as mean ± SD. *$P < 0.05$ (unpaired *t*-test). n.s., not significant, $n = 3$ mice each.

Data information: OS, outer segment; IS, inner segment; ONL, outer nuclear layer; INL, inner nuclear layer.
Source data are available online for this figure.

fusion and neurotransmitter release (Jean & Pilgrim, 2017). Excess amounts of Unc119 may affect photoreceptor synaptic function. While inhibition of rod Tα translocation from the outer segment affects synaptic transmission from rod photoreceptors to rod bipolar cells (Majumder *et al*, 2013), the scotopic b/a-wave ratio in *Klhl18*$^{+/+}$ mice was comparable with that in *Klhl18*$^{-/-}$ mice in which Tα mislocalized to the inner part of rod photoreceptors. Furthermore, a previous report showed that Unc119 suppresses rhodopsin-mediated transducin activation and dopamine D2 receptor-mediated G protein activation (Gopalakrishna *et al*, 2011). Together, the increased amounts of the Unc119 protein are also suggested to be a cause of the decreased response to light in *Klhl18*$^{-/-}$ rod photoreceptors.

Does Cul3–Klhl18 also function in cone photoreceptors? Our and other groups' data support the idea that Cul3–Klhl18 plays a significant role mainly in rod photoreceptors. Light- and dark-dependent Tα translocation between the outer segment and inner part can be observed in rod photoreceptors, but not in cone photoreceptors (Elias *et al*, 2004; Kennedy *et al*, 2004). *Klhl18* expression decreases in the *Nrl*$^{-/-}$ retina, in which the absence of rod photoreceptors is accompanied by an increased number of S-cone-like cells (Mears *et al*, 2001; Yoshida *et al*, 2004). We observed no significant differences in photopic ERG amplitudes, which mainly reflect cone photoreceptor function, between *Klhl18*$^{+/+}$ and *Klhl18*$^{-/-}$ mice.

We found that Cul3–Klhl18 recognizes Unc119 as a target protein *in vitro*, in cultured cells, and *in vivo*. *Cul3*, *Klhl18*, and *Unc119* are evolutionarily conserved from nematodes to humans. We observed the conserved interaction using plasmids encoding *C. elegans*, mouse, and human Klhl18 and Unc119. In *Drosophila* photoreceptor cells, the α-subunit of the heterotrimeric G protein, Gq, translocates from the membrane to the cytosol by light, similar to rod Tα in vertebrates (Kosloff *et al*, 2003). Modulation of G protein α subunit translocation in photoreceptors by Klhl18-mediated Unc119 ubiquitination and degradation may be a conserved mechanism among species. However, we cannot exclude the possibility that there may be other Cul3–Klhl18 target proteins modulating rod Tα translocation and/or the rod light response. Additional substrates of Cul3–Klhl18 may be identified in future studies. In addition to Tα, Tβγ also shows light- and dark-dependent translocation in rod photoreceptors, which modulates rod light responses (Kassai *et al*, 2005). We observed that inhibition of the Cul3–Klhl18 or calcineurin activity as well as Unc119 overexpression leads to the mislocalization of Tα but not Tγ to the inner part of rod photoreceptors, suggesting that regulation of rod Tβγ translocation is independent of the Cul3–Klhl18-Unc119 pathway. In the light, increased amounts of Unc119 are suggested to inhibit Tα translocation to the outer segment in rod photoreceptors. Rod Tα and Tβγ are proposed to translocate separately from the inner part to the outer segment (Constantine *et al*, 2012). PrBP/δ, encoded by *Pde6d*, contributes to Tγ translocation to the outer segment of rod photoreceptors. In the *Pde6d*$^{-/-}$ retina, Tγ mislocalizes to the inner part of rod photoreceptors, while Tα does not (Zhang *et al*, 2007). Therefore, Tα and Tβγ can be separately localized to the inner part of rod photoreceptors.

Unc119 solubilizes proteins anchored to the membrane, including Tα, by lipid modification (Gopalakrishna *et al*, 2011). It was previously reported that *Unc119*$^{-/-}$ mice show defects in Tα translocation from the inner part to the outer segment in rod photoreceptors (Zhang *et al*, 2011). This study proposed that, in the absence of Unc119, Tα is strongly anchored to membranes in the inner part of rod photoreceptors, resulting in impairment of Tα translocation from the inner part to the outer segment (Zhang *et al*, 2011). In contrast, we observed that overexpression of Unc119 causes rod Tα mislocalization to the inner part. Since about 30% of the total amount of the Unc119 protein is localized in the outer segment of photoreceptors (Sinha *et al*, 2013), excess amounts of Unc119 may abnormally extract and solubilize Tα from the outer segment membrane, leading to mislocalization of Tα to the inner part. Furthermore, a previous study showed that Unc119 overexpression inhibits transport of its cargos, Src family kinases (SFKs), to the target membrane in cultured cells (Konitsiotis *et al*, 2017). This study proposes that the Unc119 protein without loading SFKs competitively binds to Arl2/3, which are the small GTPases required for cargo release from Unc119. Binding of Arl3 to Unc119 facilitates lipidated cargo release and trafficking to cilia (Fansa & Wittinghofer,

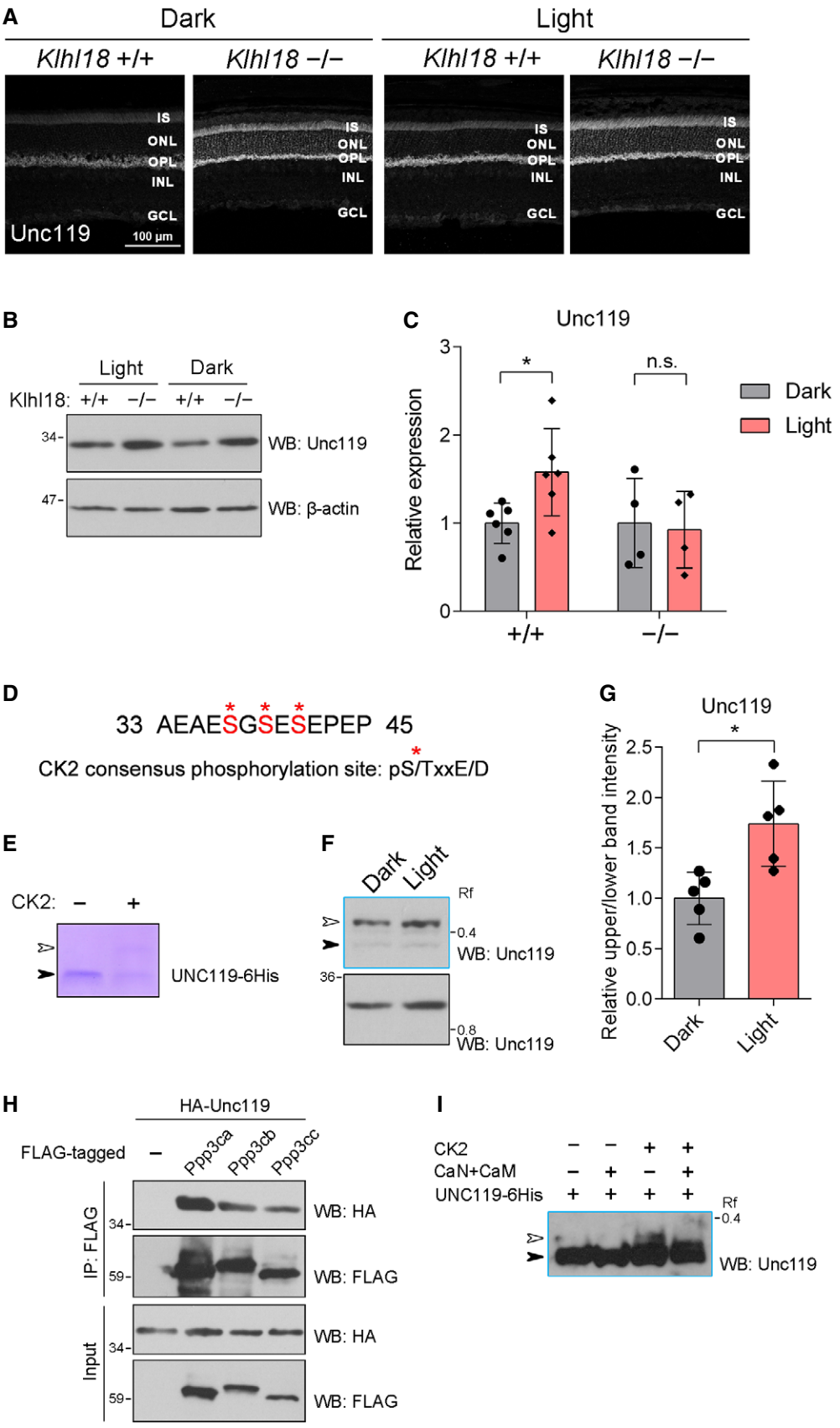

Figure 6.

Figure 6. Phosphorylation and dephosphorylation of Unc119 by CK2 and calcineurin, respectively.

A Immunostaining of retinal sections from dark- or light- (1,000 lx) adapted (4 h) *Klhl18*$^{+/+}$ and *Klhl18*$^{-/-}$ mice with an anti-Unc119 antibody. The Unc119 signal in the IS, ONL, and OPL decreased under dark condition in the *Klhl18*$^{+/+}$ retina. No obvious differences were observed between dark- and light-adapted *Klhl18*$^{-/-}$ retinas. IS, inner segment; ONL, outer nuclear layer; OPL, outer plexiform layer; INL, inner nuclear layer; GCL, ganglion cell layer.

B, C Western blot analysis of the Unc119 protein in dark- or light- (1,000 lx) adapted (4 h) *Klhl18*$^{+/+}$ and *Klhl18*$^{-/-}$ retinas. β-Actin was used as a loading control (B). Relative Unc119 protein levels in *Klhl18*$^{+/+}$ and *Klhl18*$^{-/-}$ retinas were determined by quantification of Unc119 band intensity (normalized to β-actin) (C). Relative Unc119 expression levels between dark- and light-adapted conditions were compared between *Klhl18*$^{+/+}$ (left) and *Klhl18*$^{-/-}$ (right) retinas. The averaged Unc119 expression levels under the dark-adapted condition in *Klhl18*$^{+/+}$ and *Klhl18*$^{-/-}$ retinas were set to 1.0. Data are presented as mean ± SD. *$P < 0.05$ (unpaired *t*-test). n.s., not significant. *Klhl18*$^{+/+}$; $n = 6$ mice each, *Klhl18*$^{-/-}$; $n = 4$ mice each.

D Amino acid sequence of mouse Unc119 (residues 33–45) containing predicted phosphorylation sites by CK2 (red) is shown. Asterisks indicate predicted phosphorylation sites for CK2.

E UNC119 is phosphorylated by CK2 *in vitro*. Recombinant 6xHis-tagged human UNC119 was applied to the *in vitro* kinase assay using purified human CK2. UNC119 phosphorylation was analyzed by Phos-tag SDS–PAGE. White and black arrowheads indicate upshifted (white) and native (black) bands.

F, G Light-dependent Unc119 phosphorylation in the retina. Wild-type mice were dark-adapted for 4 h or light-adapted (7,000 lx) for 15 min after dark adaptation for 4 h. The retinal lysates were analyzed by Phos-tag (blue box) and conventional (black box) Western blotting with an anti-Unc119 antibody (F). Relative phosphorylation of Unc119 was quantified by the ratio of the upper band intensity (white arrowhead) to the lower band intensity (black arrowhead) (G). Data are presented as mean ± SD. *$P < 0.05$ (unpaired *t*-test), $n = 5$ retinas from three mice each.

H Immunoprecipitation analysis of Unc119 and the catalytic subunit of calcineurin. HEK293T cells were transfected with plasmids expressing HA-tagged Unc119 and the indicated FLAG-tagged catalytic subunits of calcineurin. The cell lysates were subjected to immunoprecipitation with the anti-FLAG antibody. Immunoprecipitated proteins were analyzed by Western blotting with anti-FLAG and anti-HA antibodies.

I UNC119 is dephosphorylated by calcineurin *in vitro*. Recombinant 6xHis-tagged human UNC119 applied to the *in vitro* kinase assay using CK2 was treated with purified calcineurin and calmodulin. UNC119 phosphorylation was analyzed by Phos-tag Western blotting with an anti-Unc119 antibody. White and black arrowheads indicate upshifted (white) and native (black) bands. CaN, calcineurin; CaM, calmodulin.

Source data are available online for this figure.

2016). Therefore, the increased amount of Unc119 protein not loaded with Tα is suggested to competitively interact with Arl3, resulting in inhibition of cargo release and inefficient Tα transport to the outer segment—a specialized primary cilium.

How is Cul3–Klhl18-mediated Unc119 ubiquitination and degradation regulated? We found that Unc119 is phosphorylated by CK2 and dephosphorylated by calcineurin. Unc119 was phosphorylated more under light conditions than dark conditions. In retinal photoreceptors, intracellular Ca^{2+} concentration increases under dark-adapted conditions and decreases under light-adapted conditions (Woodruff *et al*, 2002). Therefore, we focused on the calcium- and calmodulin-dependent serine/threonine phosphatase, calcineurin, which is supposed to dephosphorylate Unc119 strongly in low light. It was previously reported that a synthetic peptide that facilitates dissociation of Tα and Tβγ can trigger transducin translocation to the inner part of photoreceptor cells (Rosenzweig *et al*, 2007; Slepak & Hurley, 2008). Dissociation of the transducin complex by this peptide does not require intra-photoreceptor Ca^{2+} concentration change. However, it is unclear whether light-dependent intra-photoreceptor Ca^{2+} concentration change without the synthetic peptide contributes to the dissociation of the transducin complex in rod outer segments. Further mechanistic studies are required to uncover whether calcineurin-mediated change in Unc119 protein levels is involved in Tα and Tβγ dissociation and subsequent transducin translocation. We observed that the amount of the phosphorylated form of Unc119 is higher than that of the unphosphorylated form in the retina by Phos-tag Western blot. Our results suggest that Cul3–Klhl18 preferentially ubiquitinates and degrades the unphosphorylated form of Unc119 over the phosphorylated form, resulting in the higher amount of the phosphorylated form of Unc119 compared with that of the unphosphorylated form. It should be noted that we do not exclude the possibility that Cul3–Klhl18-mediated Unc119 ubiquitination is also modulated by other mechanisms. For example, it was previously reported that Klhl12 and its substrate Sec31 form a complex with calcium-binding proteins, Pef1 and Alg2, and that Sec31 ubiquitination by Cul3–Klhl12 is promoted by calcium through Pef1 and Alg2 (McGourty *et al*, 2016). Although whether Klhl18 and Unc119 can interact with Pef1 and Alg2 is unknown, it is possible that Cul3–Klhl18-mediated Unc119 ubiquitination is modulated by these calcium-binding proteins. We also suppose that there may be other CK2 and calcineurin substrates involved in Unc119 protein level, Tα translocation, and/or protection of light-induced photoreceptor damage. Understanding detailed molecular mechanisms underlying the regulation of Cul3–Klhl18-mediated Unc119 ubiquitination awaits future analyses.

Light-dependent intracellular Ca^{2+} concentration change has several effects on phototransduction (Fain *et al*, 2001; Luo *et al*, 2008; Yau & Hardie, 2009). First, the activation of guanylate cyclase (GC) is facilitated by guanylate cyclase-activating proteins, which are Ca^{2+}-binding proteins that are negatively regulated by Ca^{2+} (Koch & Stryer, 1988; Palczewski *et al*, 1994, 2004; Dizhoor *et al*, 1995; Mendez *et al*, 2001; Burns *et al*, 2002). In the light, the disinhibited GC protein produces cGMP, which binds to and opens the cGMP-gated channel in photoreceptor cells. Second, rhodopsin kinase is also negatively modulated by a Ca^{2+}-binding protein called recoverin or S-modulin (Dizhoor *et al*, 1991; Kawamura & Murakami, 1991; Kawamura, 1993; Chen *et al*, 1995; Makino *et al*, 2004). Under light conditions, disinhibition of rhodopsin kinase by Ca^{2+} decrease allows rhodopsin phosphorylation and inactivation. Third, Ca^{2+}, through binding to calmodulin, reduces cGMP affinity for the cGMP-gated channel (Hsu & Molday, 1993; Chen *et al*, 1994). It remains unclear how these three mechanisms and the calcineurin-modulated Tα translocation cooperatively or independently function. Future studies to investigate crosstalk in the Ca^{2+}-mediated signaling pathways would increase our understanding of how rod photoreceptors can properly respond to a wide range of light intensities.

Vision begins with light reception by rod and cone photoreceptors, and yet light is also harmful to these photoreceptor cells. Exposure to light is a proposed risk factor for the progression of degenerative retinal diseases including AMD and RP (Parmeggiani

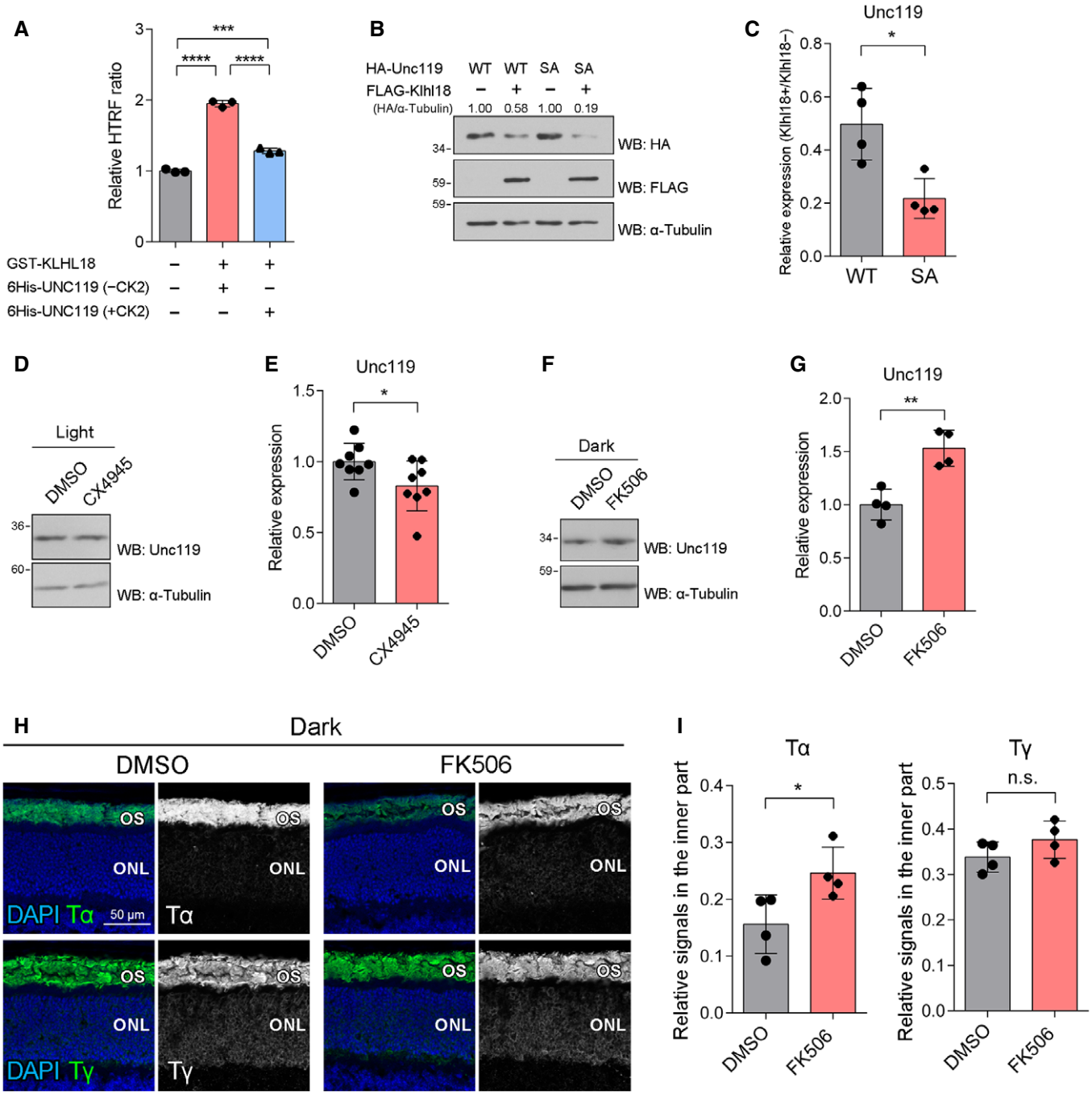

Figure 7.

et al, 2011; Marquioni-Ramella & Suburo, 2015; Schick *et al*, 2016; Mitchell *et al*, 2018). Inhibition of rod phototransduction activation can prevent retinal photoreceptor degeneration. For example, loss of rhodopsin suppresses photoreceptor damage by light (Grimm *et al*, 2000). Mice lacking the gene encoding rod arrestin ($Sag^{-/-}$) or rhodopsin kinase ($Grk1^{-/-}$), models for Oguchi disease and/or RP, show prolonged photoresponses in rod photoreceptors and increased susceptibility to light-triggered photoreceptor damage (Xu *et al*, 1997; Chen *et al*, 1999a,b; Hao *et al*, 2002). Disruption of the *Gnat1* gene encoding rod Tα suppresses the retinal degeneration observed in $Sag^{-/-}$ or $Grk1^{-/-}$ mice (Hao *et al*, 2002). Light-dependent transducin translocation from the outer segment to the inner part is suggested to decrease photoreceptor damage (Fain, 2006). Indeed, inhibition of rod Tα translocation to the inner part by amino acid substitution decreases the light-induced photoreceptor degeneration threshold (Majumder *et al*, 2013). We found that the genetic or pharmacological inactivation of Cul3–Klhl18 and calcineurin inhibitors FK506 and CsA that are widely used clinically as immunosuppressant drugs represses light-triggered photoreceptor damage, and is accompanied by increased Unc119 protein expression and

Figure 7. Klhl18-mediated Unc119 degradation is modulated by phosphorylation and dephosphorylation.

A Inhibition of Klhl18 binding to Unc119 by CK2. Recombinant GST-fused human KLHL18 and 6xHis-tagged human UNC119 with or without phosphorylation by CK2 were incubated with anti-GST-d2 and anti-6HIS-Eu Gold antibodies. The mixtures were subjected to HTRF assay, and the HTRF ratio was quantified. Data are presented as mean ± SD of triplicate samples. ***$P < 0.001$, ****$P < 0.0001$ (one-way ANOVA followed by Tukey's multiple comparisons test), $n = 3$.

B, C A plasmid expressing FLAG-tagged Klhl18 was transfected into Neuro2a cells along with a plasmid expressing HA-tagged Unc119 wild-type (WT) or S37A/S39A/S41A (SA). The cell lysates were analyzed by Western blotting with anti-HA and anti-FLAG antibodies. α-Tubulin was used as a loading control (B). Unc119 protein expression levels were determined by quantification of Unc119 band intensity (normalized to α-tubulin) and represented as $Klhl18^{+}/Klhl18^{-}$ ratios (C). Data are presented as mean ± SD. *$P < 0.05$ (unpaired t-test), $n = 4$.

D, E Western blot analysis of the Unc119 protein in the retina from CX4945-treated mice. Wild-type mice were light-adapted (7,000 lx) for 15 min after dark adaptation for 4 h. The mice were treated with CX4945 2 h before the beginning of light adaptation. Unc119 expression decreased in the retinas of CX4945-treated mice. α-Tubulin was used as a loading control (D). Relative Unc119 protein levels were determined by quantification of Unc119 band intensity (normalized to α-tubulin) (E). Data are presented as mean ± SD. *$P < 0.05$ (unpaired t-test), $n = 8$ retinas from four mice each.

F, G Western blot analysis of the Unc119 protein in the retina from FK506-treated mice. FK506 was subcutaneously injected into wild-type mice every day for 4 days. The mice were dark-adapted for 4 h before harvest. Unc119 expression increased in the retinas of FK506-treated mice. α-Tubulin was used as a loading control (F). Relative Unc119 protein levels were determined by quantification of Unc119 band intensity (normalized to α-tubulin) (G). Data are presented as mean ± SD. **$P < 0.01$ (unpaired t-test), $n = 4$ mice each.

H, I Subcellular localization of Tα and Tγ in retinal photoreceptor cells of FK506-treated mice. (H) Retinal sections obtained from dark-adapted (4 h) mice treated with FK506 were immunostained using anti-Tα and anti-Tγ antibodies. FK506 was subcutaneously injected into wild-type mice every day for 4 days. (I) The immunofluorescence signals of Tα and Tγ detected in the inner part of photoreceptors were quantified using ImageJ software. The measured signals of Tα or Tγ in the inner part of photoreceptors were expressed as a proportion to the total (OS + the inner part) signals of Tα or Tγ in photoreceptors, respectively. Data are presented as mean ± SD. The Tα signals in the inner part of photoreceptors increased in the retina of the FK506-treated mice. *$P < 0.05$, n.s., not significant (unpaired t-test), $n = 4$ mice each. OS, outer segment; ONL, outer nuclear layer.

Source data are available online for this figure.

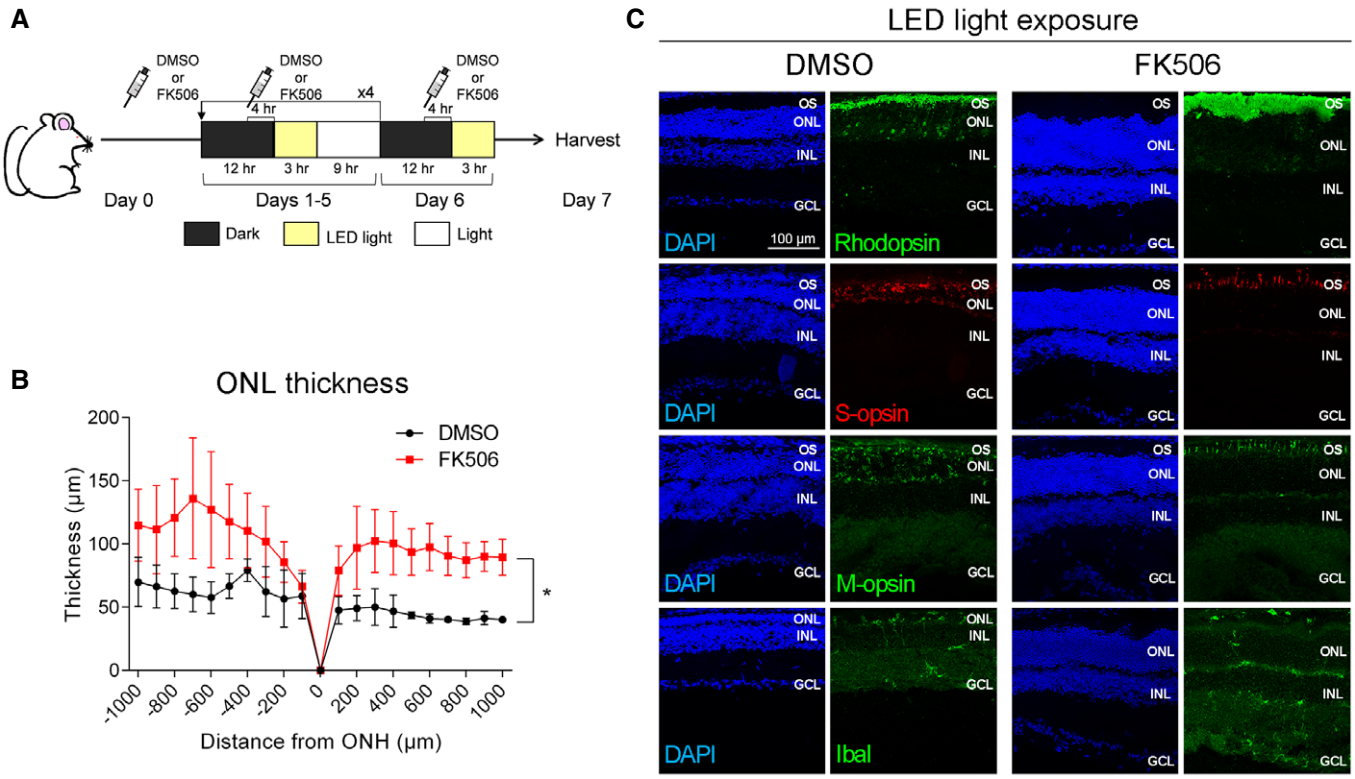

Figure 8. Calcineurin inhibition suppresses light-induced retinal degeneration.

A Experimental design for exposure of the mice treated with FK506 to LED light. FK506 was injected into mice every day for 6 days.

B Retinal sections from FK506-treated mice after light exposure were stained with DAPI, and then, the ONL thickness was measured. Data are presented as mean ± SD. *$P < 0.05$ (two-way repeated-measures ANOVA), $n = 3$ and 4 mice (DMSO and FK506, respectively). ONH, optic nerve head.

C Immunohistochemical analysis of retinas from FK506-treated mice after light exposure using marker antibodies as follows: Rhodopsin (rod outer segments), S-opsin (S-cone outer segments), M-opsin (M-cone outer segments), and Iba1 (microglia or macrophages). Nuclei were stained with DAPI (blue). Rod and cone outer segments were severely disorganized in the DMSO-injected retina. OS, outer segment; ONL, outer nuclear layer; INL, inner nuclear layer; GCL, ganglion cell layer.

mislocalization of rod Tα to the inner part of the rod photoreceptor. However, we cannot be certain that Tα mislocalization is the only cause of the decreased light-induced photoreceptor damage. The decreased light response due to the increased amount of Unc119 protein could also cause the suppression of light-induced damage. Together, Cul3–Klhl18 inactivation and calcineurin inhibitors may be applicable to preserve the retina in normal and disease conditions by protecting it from light-induced damage.

Materials and Methods

Animal care

All procedures conformed to the ARVO statement for the Use of Animals in Ophthalmic and Vision Research. These procedures were approved by the Institutional Safety Committee on Recombinant DNA Experiments (approval ID 4220) and Animal Experimental Committees of the Institute for Protein Research (approval ID 29-01-2) at Osaka University and were performed in compliance with the institutional guidelines. Mice were housed in a temperature-controlled room at 22°C with a 12-h light/dark cycle. Fresh water and rodent diet were available at all times. All animal experiments were performed with mice of either sex.

Generation of *Klhl18*$^{-/-}$ mice

A targeting vector (PRPGS00036_C_D09) obtained from the Knockout Mouse Project (KOMP), in which the LacZ, neomycin-resistant (Neo) gene cassettes, and *loxP* sites were inserted in the genomic region of *Klhl18*, was linearized and transfected into the JM8A3 embryonic stem (ES) cell line (Pettitt *et al*, 2009). The culture, electroporation, and selection of ES cells were performed as described previously (Muranishi *et al*, 2011). ES cells that were heterozygous for the targeted gene disruption were microinjected into C57BL/6 blastocysts to obtain chimeric mice. We obtained *Klhl18*$^{-/-}$ mice by crossing the *Klhl18* flox mouse line with the *CAG-Cre* transgenic mouse line, which expresses Cre recombinase under control of the *CAG* promoter (Sakai & Miyazaki, 1997). The *rd8* mutation carried in the C57BL/6N strain (Mattapallil *et al*, 2012) was removed by outcrossing with C57BL/6J mice before experiments. To compare photoreceptor susceptibility to light-induced damage, *Klhl18*$^{+/-}$ or *Klhl18*$^{-/-}$ mice were backcrossed with Balb/c mice to generate albino *Klhl18*$^{+/+}$ and *Klhl18*$^{-/-}$ mice homozygous for the variant encoding Leu450 in the *Rpe65* gene (Wenzel *et al*, 2001). Primer sequences for genotyping are listed in Table EV1.

Chemicals

MG132 was purchased from Millipore. MLN4924 for use in cultured cells was obtained from Active Biochem. MLN4924 for use in mice was obtained from Chemscene. CX4945 was purchased from Selleckchem. FK506 and CsA were obtained from Abcam.

Cell culture and transfection

HEK293T and Neuro2a cells were cultured in DMEM (Sigma) containing 10% fetal bovine serum supplemented with penicillin (100 μg/ml) and streptomycin (100 μg/ml) at 37°C with 5% CO_2. Transfection was carried out with the calcium phosphate method for HEK293T cells or with Lipofectamine LTX (Invitrogen) for Neuro2a cells.

RT–PCR and qRT–PCR analyses

RT–PCR and qRT–PCR analyses were performed as described previously (Chaya *et al*, 2014; Okamoto *et al*, 2017). Total RNAs were extracted using TRIzol (Ambion) from tissues dissected from ICR mice at 4 weeks, retinas from *Klhl18*$^{+/+}$ and *Klhl18*$^{-/-}$ mice at 1 M, and retinas from *Pde6b*$^{+/+}$ and *Pde6b*$^{rd1/rd1}$ mice at P14. Total RNA of 0.5 or 2 μg was reverse-transcribed into cDNA with random hexamers using SuperscriptII (Invitrogen) or PrimeScriptII Reagent (TaKaRa). The cDNAs were used for PCR by rTaq polymerase (TaKaRa). Primer sequences used for amplification are listed in Table EV1. qRT–PCR was performed using SYBR Green ER Q-PCR Super Mix (Invitrogen) and Thermal Cycler Dice Real Time System Single MRQ TP870 (Takara) according to the manufacturer's protocols. Quantification was performed by Thermal Cycler Dice Real Time System software ver. 2.0 (Takara). Primer sequences used for amplification are listed in Table EV1.

In situ hybridization

In situ hybridization was performed as described previously (Tsutsumi *et al*, 2018). Mouse embryos and eye cups were fixed using 4% paraformaldehyde (PFA) in phosphate-buffered saline (PBS) overnight at 4°C. The tissues were then equilibrated in 30% sucrose in PBS overnight at 4°C, embedded in TissueTec OCT compound 4583 (Sakura, Japan), and frozen. Alternatively, mouse eye balls were freshly frozen. Digoxigenin-labeled anti-sense and sense riboprobes for mouse *Klhl18* and *Ppp3cc* were synthesized by *in vitro* transcription using 11-digoxigenin UTPs (Roche). The sense probes were used as a control. *Klhl18* and *Ppp3cc* cDNA fragments for *in situ* hybridization probes were generated by RT–PCR using mouse retinal cDNA as templates. Primer sequences used for amplification are listed in Table EV1.

ERG recording

Electroretinograms (ERGs) were recorded as described previously (Omori *et al*, 2015). In brief, mice were dark-adapted overnight and then anesthetized with an intraperitoneal injection of 100 mg/kg ketamine and 10 mg/kg xylazine diluted in saline (Otsuka). Pupils were dilated with topical 0.5% tropicamide and 0.5% phenylephrine HCl. ERG responses were measured by the PuREC system with LED electrodes (Mayo Corporation). The mice were placed on a heating pad and stimulated with an LED flash. Four levels of stimulus intensities ranging from −4.0 to 1.0 log cd s/m^2 were used for the scotopic ERGs. After mice were light adapted for 10 min, the photopic ERGs were recorded on a rod-suppressing white background of 1.3 log cd s/m^2. Four levels of stimulus intensities ranging from −0.5 to 1.0 log cd s/m^2 were used for the photopic ERGs. Eight responses at −4.0 log cd s/m^2 and four responses at −3.0 log cd s/m^2 were averaged for scotopic recordings. Sixteen responses were averaged for photopic recordings.

Immunofluorescent analysis of retinal sections

Immunohistochemical analysis of retinal sections was performed as described previously (Omori *et al*, 2010). Mouse eyes or eye cups were fixed with 4% PFA in PBS for 15 s to 30 min at room temperature. The samples were rinsed in PBS followed by cryoprotection using 30% sucrose in PBS overnight at 4°C, embedded in TissueTec OCT compound 4583 (Sakura), frozen, and sectioned. Frozen 20-μm sections on slides were dried for more than 3 h at room temperature, rehydrated in PBS for 5 min, incubated with blocking buffer (5% normal donkey serum, and 0.1% Triton X-100 in PBS) for 30 min, and then with primary antibodies for 4 h at room temperature or overnight at 4°C. Slides were washed with PBS three times for 5 min each time and incubated with fluorescent dye-conjugated secondary antibodies and DAPI (1:1,000, Nacalai Tesque) for 2 h at room temperature while shielded from light. The sections were coverslipped with gelvatol after being washed with PBS three times. The specimens were observed under a laser confocal microscope (LSM700, Carl Zeiss). Primary antibodies used in this study were as follows: rabbit anti-Tα (1:500, Santa Cruz, sc-389), rabbit anti-Tγ (1:500, Santa Cruz, sc-373), rabbit anti-visual arrestin (1:500, Affinity BioReagents, PA1-731), rabbit anti-Rhodopsin (1:2,500, LSL, LB-5597), mouse anti-Rom1 (1:250, a kind gift from Dr. R. Molday, University of British Columbia) (Bascom *et al*, 1992), goat anti-S-opsin (1:500, Santa Cruz, sc-14363), rabbit anti-M-opsin (1:500, Millipore, AB5405), rabbit anti-Chx10 (1:200) (Koike *et al*, 2007), mouse anti-Pax6 (1:100, DSHB), rabbit anti-Calbindin (1:1,000, Calbiochem, PC253L), mouse anti-Brn3a (1:100, Chemicon, MAB1585), mouse anti-S100β (1:2,500, Sigma, S-2532), rabbit anti-IbaI (1:500, WAKO, 019-19741), guinea pig anti-Klhl18 (1:100, generated in this study), mouse anti-Unc119 (1:10, a kind gift from Dr. F. Haeseleer, University of Washington) (Haeseleer, 2008), and guinea pig anti-Unc119 (1:200, generated in this study). We used Cy3-conjugated (1:500, Jackson ImmunoResearch Laboratories) and Alexa Fluor 488-conjugated (1:500, Sigma) secondary antibodies. Immunofluorescence signal intensities were measured and quantified using National Institutes of Health (NIH) ImageJ software. The signals for Tα or Tγ in the inner part of the photoreceptors were normalized for the total (OS + the inner part) signals for Tα or Tγ in photoreceptors, respectively, as described previously (Kassai *et al*, 2005; Rosenzweig *et al*, 2007).

Toluidine blue staining

Toluidine blue staining of retinal sections was performed as described previously (Chaya *et al*, 2017). Retinal sections were rinsed with PBS and then stained with 0.1% toluidine blue in PBS for 1 min. After washing with PBS, slides were covered with cover slips and immediately observed under the microscope.

Drug administration

MLN4924 or CX4945 dissolved in DMSO (100 mg/ml or 10 mM, respectively) was diluted in saline. FK506 dissolved in DMSO (20 mg/ml) was diluted in saline containing 10% ethanol. CsA dissolved in DMSO (200 mg/ml) was diluted in sunflower seed oil (Sigma). 60 mg/kg of MLN4924, 10 mg/kg of FK506, or 100 mg/kg of CsA was administered to mice every day by subcutaneous injection. 20 mg/kg of CX4945 was administered to mice by intraperitoneal injection. C57BL/6J mice were used to observe the subcellular localization of Tα or Tγ.

Exposure to LED light

Exposure of mice to LED light was repeated for 3 or 6 days as described previously with some modifications (Nakamura *et al*, 2018). After dark adaptation for 12 or 24 h (day 1) or 12 h (from day 2), mouse pupils were dilated with 1% cyclopentolate hydrochloride eye drops (Santen Pharmaceuticals, Osaka, Japan) 30 min before exposure to LED light (~ 450 nm). Non-anesthetized mice were exposed to ~ 7,000 lx LED light for 3 h in a mirrored device separated individually by clear partitions for the reflection of light. Ambient temperature during the light exposure was maintained at 25 ± 1.5°C. After exposure to LED light, the mice were returned to cages and housed in normal light conditions for 9 h before the next dark adaptation. After the last exposure to LED light, the mice were returned to cages and housed in the normal 12-h dark/light cycle. At day 7, ERG recordings and/or retinal dissection were performed. *Klhl18*$^{+/-}$ or *Klhl18*$^{-/-}$ mice were backcrossed with Balb/c mice to generate albino *Klhl18*$^{+/+}$ and *Klhl18*$^{-/-}$ mice homozygous for the variant encoding Leu450 in the *Rpe65* gene, which were used for the experiment (Wenzel *et al*, 2001). Balb/c mice treated with MLN4924, FK506, or CsA were also subjected to the experiment. Although mouse rhodopsin has an absorption maximum of 502 nm (Imai *et al*, 2007), light with a wavelength of 403 ± 10 nm causes rhodopsin-mediated photoreceptor damage (Grimm *et al*, 2001).

Plasmid constructs

A full-length cDNA fragment of mouse *Klhl18* was amplified by PCR using mouse retinal cDNA as a template and subcloned into the pCAGGSII-3xFLAG, pCAGGSII-2xHA (Irie *et al*, 2015), and pCAGGSII (Omori *et al*, 2010) vectors. The cDNA fragments encoding the Klhl18-N and Klhl18-C were amplified by PCR using the plasmid encoding full-length Klhl18. A full-length cDNA fragment of mouse *Unc119* was amplified by PCR using mouse retinal cDNA as a template, and subcloned into the pCAGGSII-3xFLAG and pCAGGSII-2xHA vectors. *3xFLAG-Unc119* digested from pCAGGSII-3xFLAG-Unc119 was ligated into the pCIG vector (Matsuda & Cepko, 2004). The Unc119 S37A/S39A/S41A mutation was introduced by site-directed mutagenesis by PCR. Full-length cDNA fragments of *C. elegans kel-3* and *unc-119* were amplified by PCR using *C. elegans* cDNA as a template, and subcloned into the pCAGGSII-3xFLAG and pCAGGSII-2xHA vectors, respectively. To construct N-terminal GST-fused human KLHL18, a full-length cDNA fragment of human *KLHL18* was amplified by PCR using a human KLHL18 clone purchased from DNAFORM (Clone ID: 100002137) as a template and subcloned into the pGEX-4T-3 vector (GE Healthcare). To construct N- or C-terminal 6xHis-tagged human UNC119, a full-length cDNA fragment of human *UNC119* was amplified by PCR using a human UNC119 clone obtained from PlasmID (cloneID: HsCD00330844) as a template and subcloned into the pET-28b vector (Novagen). The human UNC119 S37A/S39A/S41A mutation was introduced by site-directed mutagenesis by PCR. The cDNA fragment encoding full-length of Ubiquitin was amplified by PCR

using mouse retinal cDNA as a template and subcloned into the pCAGGSII-6xHis vector, which was modified from the pCAGGSII vector. Full-length cDNA fragments of mouse *Unc119b*, *Ppp3ca*, *Ppp3cb*, and *Ppp3cc* were amplified by PCR using mouse retinal cDNA as a template and subcloned into the pCAGGSII-3xFLAG vector. Primer sequences used for amplification are listed in Table EV1.

Immunoprecipitation assay

Immunoprecipitation assay was performed as described previously (Kozuka *et al*, 2017). HEK293T cells were transfected with plasmids expressing FLAG-tagged proteins and other expression plasmids. At 48 h after transfection, the cells were lysed in a lysis buffer supplemented with protease inhibitors (20 mM Tris–HCl pH 7.4, 150 mM NaCl, 1% Nonidet P-40 (NP-40), 1 mM EDTA, 1 mM PMSF, 2 μg/ml leupeptin, 5 μg/ml aprotinin, and 3 μg/ml pepstatin A) and centrifuged at 15,100 *g* for 5 min twice. The supernatants were incubated with an anti-FLAG M2 affinity gel (Sigma-Aldrich) overnight at 4°C. After washing five times with wash buffer (20 mM Tris–HCl pH 7.4, 150 mM NaCl, 1% NP-40, and 1 mM EDTA), bound proteins were eluted with elution buffer (20 mM Tris–HCl pH 7.4, 150 mM NaCl, 5 mg/ml 1 × FLAG peptide) in a 30 min of incubation at 4°C or with SDS-sample buffer. The supernatants were incubated with SDS-sample buffer for 30 min at room temperature.

Western blot analysis

Western blot analysis was performed as described previously (Ueno *et al*, 2018). HEK293T and Neuro2a cells were washed with PBS twice and lysed in a lysis buffer supplemented with protease inhibitors (buffer A: 20 mM Tris–HCl pH 7.4, 150 mM NaCl, 1% NP-40, 1 mM EDTA, 1 mM PMSF, 2 μg/ml leupeptin, 5 μg/ml aprotinin, and 3 μg/ml pepstatin A). Mouse retinas were lysed in a SDS-sample buffer, in buffer A or in buffer B (20 mM Tris–HCl pH 7.4, 150 mM NaCl, 1% NP-40 supplemented with phosphatase inhibitor cocktail (Roche)). Samples were resolved by SDS–PAGE and transferred to PVDF membranes (Millipore) using a semidry transfer cell (Bio-Rad). The membranes were blocked with blocking buffer (3% skim milk, and 0.05% Tween 20 in Tris-buffered saline (TBS)) and incubated with primary antibodies overnight at 4°C. The membranes were washed with 0.05% Tween 20 in TBS three times for 10 min each and then incubated with secondary antibodies for 2 h at room temperature. Signals were detected using Chemi-Lumi One L (Nacalai) or Pierce Western Blotting Substrate Plus (Thermo Fisher Scientific). We used the following primary antibodies: mouse anti-FLAG M2 (1:5,000, Sigma, F1804), rabbit anti-FLAG (1:5,000, Sigma, F7425), rat anti-HA (1:2,500 or 1:5,000, Santa Cruz, sc-805), mouse anti-6xHis (1:6,000, Roche, 04 905 318 001), mouse anti-6xHis (1:6,000, Nacalai, 04428-26), mouse anti-GST (1:8,000, Nacalai, 04559-74), mouse anti-β-actin (1:5,000, Sigma, A5316), mouse anti-α-tubulin (Cell Signaling, DM1A, 1:5,000, T9026), guinea pig anti-Klhl18 (1:200, generated in this study), mouse anti-Unc119 (1:100, a kind gift from Dr. F. Haeseleer, University of Washington), and guinea pig anti-Unc119 (1:125, 1:250 or 1:500, generated in this study) antibodies. The following secondary antibodies were used: horseradish peroxidase-conjugated anti-mouse IgG (1:10,000, Zymed), anti-guinea pig IgG (1:10,000, Jackson Laboratory), and anti-rabbit IgG (1:10,000, Jackson Laboratory). Phosphorylated Unc119 was detected by 8% SDS–PAGE with 20 or 50 μM Phos-tag acrylamide (FUJIFILM Wako) or by SDS–PAGE with SuperSep Phos-tag 50 μM, 7.5% (FUJIFILM Wako) according to the manufacturer's instruction (Kinoshita *et al*, 2006; Kinoshita & Kinoshita-Kikuta, 2011). The band intensity was quantified with NIH ImageJ software.

Antibody production

Antibody production was performed as described previously (Omori *et al*, 2017). Briefly, cDNA fragments encoding a middle portion of mouse Klhl18 (residues 210–285) and full-length mouse Unc119 were amplified by PCR and subcloned into the pGEX-4T-3 plasmid (GE Healthcare). The GST-fused Klhl18 or Unc119 protein was expressed in *Escherichia coli* strain BL21 (DE3) and purified with glutathione Sepharose 4B (GE Healthcare). An antibody against Klhl18 or Unc119 was obtained by immunizing guinea pigs with the purified GST-fused Klhl18 or Unc119 protein.

Protein purification

GST and GST-fused human KLHL18 proteins were expressed and purified from *E. coli* strain BL21 (DE3). Cells were grown in LB medium to $OD_{600\ nm}$ 0.6 followed by treatment with 1 mM isopropyl β-d-thiogalactopyranoside (IPTG) at 25°C for 4 h and harvest by centrifugation. Harvested cells were lysed in sonication buffer (100 mM EDTA, 1% Triton X-100, and 1 mM DTT in PBS supplemented with 1 mM PMSF, 2 μg/ml leupeptin, 5 μg/ml aprotinin, and 3 μg/ml pepstatin A) and centrifuged. The supernatants were mixed with glutathione Sepharose 4B (GE Healthcare) and incubated for 2 h at room temperature. The beads were washed with wash buffer (20 mM Tris–HCl pH 7.4, 1% NP-40, 150 mM NaCl, and 5 mM EDTA) and eluted with elution buffer (40 mM glutathione, 200 mM NaCl, 100 mM Tris–HCl, pH 9.0, 0.1% Triton X-100, and 1 mM DTT). 6xHis-tagged human UNC119 protein was expressed and purified from *E. coli* strain BL21 (DE3). Cells were grown in LB medium to $OD_{600\ nm}$ 0.6 followed by treatment with 1 mM IPTG at 25°C for 3.5 h and harvest by centrifugation. Harvested cells were lysed in sonication buffer (20 mM Tris–HCl pH 7.4, 1 mM EDTA, 150 mM NaCl, 1% Triton X-100, 1 mM DTT, 50 mM imidazole, 1 mM PMSF, 2 μg/ml leupeptin, 5 μg/ml aprotinin, and 3 μg/ml pepstatin A) and centrifuged. The supernatants were mixed with Ni-NTA Agarose (QIAGEN) and incubated at 4°C for 2 h. The beads were washed with sonication buffer and eluted with elution buffer (200 mM imidazole, 150 mM NaCl, 20 mM Tris–HCl, pH 7.4, 0.1% Triton X-100, and 1 mM DTT).

GST pull-down assay

Three micrograms of the purified 6xHis-tagged human UNC119 was incubated with 3 μg of the purified GST or GST-fused human KLHL18 in binding buffer (0.1% NP-40, 0.5 mM DTT, 10% glycerol, 1 mM PMSF in PBS) at 30°C for 60 min, followed by a 2 h of incubation with glutathione Sepharose 4B at room temperature. The beads were washed with binding buffer five times and incubated with SDS-sample buffer for 30 min at room temperature.

HTRF assay

HTRF assay (Cisbio) was performed according to the manufacturer's instruction. The purified proteins were diluted in Epigeneous Binding Domain Detection Buffer #1(En) (Cisbio) to 2,000 nM. To observe KLHL18 binding to UNC119, 5 μl of GST-fused human KLHL18, 5 μl of 6xHis-tagged human UNC119, 5 μl of 1× anti-GST-d2 antibody (Cisbio), and 5 μl of 1× anti-6HIS-Eu Gold antibody (Cisbio) were added into a 384-well low volume white round bottom plate (Corning). After incubation at room temperature for 4 h, the 620- and 665-nm fluorescence signals were read (CLARIOstar, BMG Labtech) and the HTRF ratio (665 nm/620 nm × 10^4) was calculated. To observe CK2 effects on Klhl18 binding to Unc119, 2.78 μg of the purified 6xHis-tagged human UNC119 was incubated with 460 units of human CK2 (NEB) in 1× NEBuffer for Protein Kinase (NEB) containing 800 μM ATP at 30°C for 2 h, diluted in Epigeneous Binding Domain Detection Buffer #1(En) to 2,000 nM, and subjected to HTRF assay as described above.

Ubiquitination assay in cells

Neuro2a cells were co-transfected with plasmids encoding Klhl18, HA-tagged Unc119, and 6xHis-tagged ubiquitin. After 48 h, the cells were lysed in lysis buffer (8 M urea, 20 mM Tris–HCl pH 7.4, 500 mM NaCl, and 5 mM imidazole), sonicated, and centrifuged at 15,100 *g* for 5 min twice. The supernatants were incubated with Ni-NTA Agarose (QIAGEN) overnight at 4°C. After washing five times with lysis buffer, bound proteins were eluted with equal volume of 2× SDS-sample buffer containing 500 mM imidazole for 30 min at room temperature.

In vivo electroporation

In vivo electroporation was performed on the P0 mouse retina as described previously (Watanabe *et al*, 2015). Plasmids in 0.3 μl of PBS at a concentration of 5 μg/μl were injected into subretinal spaces of the P0 mouse followed by *in vivo* electroporation. The electroporated retinas were harvested at 1 M.

In vitro kinase assay

Two micrograms of the purified 6xHis-tagged human UNC119 were incubated with 50 or 100 units of CK2 (NEB) in 1× NEBuffer for Protein Kinase (NEB) containing 40 or 80 μM ATP at 30°C for 30 min. Reaction products were subjected to Phos-tag SDS–PAGE and Coomassie Brilliant Blue staining or Western blot.

In vitro phosphatase assay

Six micrograms of the purified 6xHis-tagged human UNC119 were incubated with 125 units of CK2 (NEB) in 1× NEBuffer for Protein Kinase (NEB) containing 100 μM ATP at 30°C for 30 min. The reaction products were next incubated with 0.5 μg of PPP3CC (Abnova), 0.5 μg of calmodulin (EMD Millipore), and 0.5 μg of CNB (Novoprotein) in phosphatase buffer (50 mM Tris–HCl pH 7.5, 1 mM $CaCl_2$, 100 mM NaCl, 0.025% NP-40, and 1 mM DTT) at 37°C for 2 h and then subjected to Phos-tag SDS–PAGE and Western blot analysis.

Statistical analysis

Data are represented as mean ± SD. Statistical analysis was performed using unpaired *t*-test, one-way ANOVA, or two-way repeated-measures ANOVA as indicated in Figure legends. A value of $P < 0.05$ was taken to be statistically significant.

Expanded View for this article is available online.

Acknowledgements
We thank F. Haeseleer and R. Molday for providing an anti-Unc119 antibody and an anti-Rom1 antibody, respectively, K. D. Kimura for providing *C. elegans* larvae, S. Kawamura, S. Ueno, S. Tachibanaki, and R. Sanuki for helpful comments, H. Hara for help with the light exposure experiments, and M. Kadowaki, A. Tani, A. Ishimaru, Y. Tohjima, K. Hasegawa, T. Tsujii, T. Nakayama, H. Abe, Y. Sasaki, Y. Omori, S. Watanabe, S. Mikusa, K. Fukunaga, S. Kubo, A. Ueno, T. Miyata, and S. Kennedy for technical assistance. This work was supported by CREST from Japan Agency for Medical Research and Development (AMED), Grant-in-Aid for Scientific Research (B) (18H02593), and Young Scientists (B) (17K15548) from the Japan Society for the Promotion of Science (JSPS), The Takeda Science Foundation, The Uehara Memorial Foundation, Senri Life Science Foundation, KANAE Foundation for the Promotion of Medical Science, The Cell Science Research Foundation, Suzuken Memorial Foundation, and Mitsui Sumitomo Insurance Welfare Foundation.

Author contributions
TC and TF designed the project. TC and TF generated *Klhl18*$^{-/-}$ mice. TC, RT, LRV, YM, and SY performed histological and molecular biological experiments. TC, RT, YM, SY, and LRV carried out biochemical experiments. TC, LRV, and SY performed ERG experiments. TC, RT, YM, and SY carried out *in vivo* electroporation. LRV and TC performed light-induced damage experiments. TC and TF wrote the manuscript. TF supervised the project.

Conflict of interest
The authors declare that they have no conflict of interest.

References

Bascom RA, Manara S, Collins L, Molday RS, Kalnins VI, McInnes RR (1992) Cloning of the cDNA for a novel photoreceptor membrane protein (rom-1) identifies a disk rim protein family implicated in human retinopathies. *Neuron* 8: 1171 – 1184

Baylor DA, Lamb TD, Yau KW (1979) Responses of retinal rods to single photons. *J Physiol* 288: 613 – 634

Blom N, Gammeltoft S, Brunak S (1999) Sequence and structure-based prediction of eukaryotic protein phosphorylation sites. *J Mol Biol* 294: 1351 – 1362

Brann MR, Cohen LV (1987) Diurnal expression of transducin mRNA and translocation of transducin in rods of rat retina. *Science* 235: 585 – 587

Broekhuyse RM, Tolhuizen EF, Janssen AP, Winkens HJ (1985) Light induced shift and binding of S-antigen in retinal rods. *Curr Eye Res* 4: 613 – 618

Burns ME, Mendez A, Chen J, Baylor DA (2002) Dynamics of cyclic GMP synthesis in retinal rods. *Neuron* 36: 81 – 91

Calvert PD, Strissel KJ, Schiesser WE, Pugh EN Jr, Arshavsky VY (2006) Light-driven translocation of signaling proteins in vertebrate photoreceptors. *Trends Cell Biol* 16: 560 – 568

Chaya T, Omori Y, Kuwahara R, Furukawa T (2014) ICK is essential for cell type-specific ciliogenesis and the regulation of ciliary transport. *EMBO J* 33: 1227 – 1242

Chaya T, Matsumoto A, Sugita Y, Watanabe S, Kuwahara R, Tachibana M, Furukawa T (2017) Versatile functional roles of horizontal cells in the retinal circuit. *Sci Rep* 7: 5540

Chen TY, Illing M, Molday LL, Hsu YT, Yau KW, Molday RS (1994) Subunit 2 (or beta) of retinal rod cGMP-gated cation channel is a component of the 240-kDa channel-associated protein and mediates Ca(2+)-calmodulin modulation. *Proc Natl Acad Sci USA* 91: 11757 – 11761

Chen CK, Inglese J, Lefkowitz RJ, Hurley JB (1995) Ca(2+)-dependent interaction of recoverin with rhodopsin kinase. *J Biol Chem* 270: 18060 – 18066

Chen CK, Burns ME, Spencer M, Niemi GA, Chen J, Hurley JB, Baylor DA, Simon MI (1999a) Abnormal photoresponses and light-induced apoptosis in rods lacking rhodopsin kinase. *Proc Natl Acad Sci USA* 96: 3718 – 3722

Chen J, Simon MI, Matthes MT, Yasumura D, LaVail MM (1999b) Increased susceptibility to light damage in an arrestin knockout mouse model of Oguchi disease (stationary night blindness). *Invest Ophthalmol Vis Sci* 40: 2978 – 2982

Constantine R, Zhang H, Gerstner CD, Frederick JM, Baehr W (2012) Uncoordinated (UNC)119: coordinating the trafficking of myristoylated proteins. *Vision Res* 75: 26 – 32

Dhanoa BS, Cogliati T, Satish AG, Bruford EA, Friedman JS (2013) Update on the Kelch-like (KLHL) gene family. *Hum Genomics* 7: 13

Dizhoor AM, Ray S, Kumar S, Niemi G, Spencer M, Brolley D, Walsh KA, Philipov PP, Hurley JB, Stryer L (1991) Recoverin: a calcium sensitive activator of retinal rod guanylate cyclase. *Science* 251: 915 – 918

Dizhoor AM, Olshevskaya EV, Henzel WJ, Wong SC, Stults JT, Ankoudinova I, Hurley JB (1995) Cloning, sequencing, and expression of a 24-kDa Ca(2+)-binding protein activating photoreceptor guanylyl cyclase. *J Biol Chem* 270: 25200 – 25206

Elias RV, Sezate SS, Cao W, McGinnis JF (2004) Temporal kinetics of the light/dark translocation and compartmentation of arrestin and alpha-transducin in mouse photoreceptor cells. *Mol Vis* 10: 672 – 681

Fain GL, Matthews HR, Cornwall MC, Koutalos Y (2001) Adaptation in vertebrate photoreceptors. *Physiol Rev* 81: 117 – 151

Fain GL (2006) Why photoreceptors die (and why they don't). *BioEssays* 28: 344 – 354

Fansa EK, Wittinghofer A (2016) Sorting of lipidated cargo by the Arl2/Arl3 system. *Small GTPases* 7: 222 – 230

Genschik P, Sumara I, Lechner E (2013) The emerging family of CULLIN3-RING ubiquitin ligases (CRL3s): cellular functions and disease implications. *EMBO J* 32: 2307 – 2320

Gopalakrishna KN, Doddapuneni K, Boyd KK, Masuho I, Martemyanov KA, Artemyev NO (2011) Interaction of transducin with uncoordinated 119 protein (UNC119): implications for the model of transducin trafficking in rod photoreceptors. *J Biol Chem* 286: 28954 – 28962

Grimm C, Wenzel A, Hafezi F, Yu S, Redmond TM, Reme CE (2000) Protection of Rpe65-deficient mice identifies rhodopsin as a mediator of light-induced retinal degeneration. *Nat Genet* 25: 63 – 66

Grimm C, Wenzel A, Williams T, Rol P, Hafezi F, Reme C (2001) Rhodopsin-mediated blue-light damage to the rat retina: effect of photoreversal of bleaching. *Invest Ophthalmol Vis Sci* 42: 497 – 505

Haeseleer F (2008) Interaction and colocalization of CaBP4 and Unc119 (MRG4) in photoreceptors. *Invest Ophthalmol Vis Sci* 49: 2366 – 2375

Hao W, Wenzel A, Obin MS, Chen CK, Brill E, Krasnoperova NV, Eversole-Cire P, Kleyner Y, Taylor A, Simon MI *et al* (2002) Evidence for two apoptotic pathways in light-induced retinal degeneration. *Nat Genet* 32: 254 – 260

Hornbeck PV, Zhang B, Murray B, Kornhauser JM, Latham V, Skrzypek E (2015) PhosphoSitePlus, 2014: mutations, PTMs and recalibrations. *Nucleic Acids Res* 43: D512 – D520

Hsu YT, Molday RS (1993) Modulation of the cGMP-gated channel of rod photoreceptor cells by calmodulin. *Nature* 361: 76 – 79

Imai H, Kefalov V, Sakurai K, Chisaka O, Ueda Y, Onishi A, Morizumi T, Fu Y, Ichikawa K, Nakatani K *et al* (2007) Molecular properties of rhodopsin and rod function. *J Biol Chem* 282: 6677 – 6684

Irie S, Sanuki R, Muranishi Y, Kato K, Chaya T, Furukawa T (2015) Rax homeoprotein regulates photoreceptor cell maturation and survival in association with Crx in the postnatal mouse retina. *Mol Cell Biol* 35: 2583 – 2596

Jean F, Pilgrim D (2017) Coordinating the uncoordinated: UNC119 trafficking in cilia. *Eur J Cell Biol* 96: 643 – 652

Kassai H, Aiba A, Nakao K, Nakamura K, Katsuki M, Xiong WH, Yau KW, Imai H, Shichida Y, Satomi Y *et al* (2005) Farnesylation of retinal transducin underlies its translocation during light adaptation. *Neuron* 47: 529 – 539

Kawamura S, Murakami M (1991) Calcium-dependent regulation of cyclic GMP phosphodiesterase by a protein from frog retinal rods. *Nature* 349: 420 – 423

Kawamura S (1993) Rhodopsin phosphorylation as a mechanism of cyclic GMP phosphodiesterase regulation by S-modulin. *Nature* 362: 855 – 857

Keeler CE (1924) The inheritance of a retinal abnormality in white mice. *Proc Natl Acad Sci USA* 10: 329 – 333

Kennedy MJ, Dunn FA, Hurley JB (2004) Visual pigment phosphorylation but not transducin translocation can contribute to light adaptation in zebrafish cones. *Neuron* 41: 915 – 928

Kerov V, Rubin WW, Natochin M, Melling NA, Burns ME, Artemyev NO (2007) N-terminal fatty acylation of transducin profoundly influences its localization and the kinetics of photoresponse in rods. *J Neurosci* 27: 10270 – 10277

Kerov V, Artemyev NO (2011) Diffusion and light-dependent compartmentalization of transducin. *Mol Cell Neurosci* 46: 340 – 346

Kinoshita E, Kinoshita-Kikuta E, Takiyama K, Koike T (2006) Phosphate-binding tag, a new tool to visualize phosphorylated proteins. *Mol Cell Proteomics* 5: 749 – 757

Kinoshita E, Kinoshita-Kikuta E (2011) Improved Phos-tag SDS-PAGE under neutral pH conditions for advanced protein phosphorylation profiling. *Proteomics* 11: 319 – 323

Klee CB, Crouch TH, Krinks MH (1979) Calcineurin: a calcium- and calmodulin-binding protein of the nervous system. *Proc Natl Acad Sci USA* 76: 6270 – 6273

Klee CB, Ren H, Wang X (1998) Regulation of the calmodulin-stimulated protein phosphatase, calcineurin. *J Biol Chem* 273: 13367 – 13370

Koch KW, Stryer L (1988) Highly cooperative feedback control of retinal rod guanylate cyclase by calcium ions. *Nature* 334: 64 – 66

Koike C, Nishida A, Ueno S, Saito H, Sanuki R, Sato S, Furukawa A, Aizawa S, Matsuo I, Suzuki N *et al* (2007) Functional roles of Otx2 transcription factor in postnatal mouse retinal development. *Mol Cell Biol* 27: 8318 – 8329

Konitsiotis AD, Rossmannek L, Stanoev A, Schmick M, Bastiaens PIH (2017) Spatial cycles mediated by UNC119 solubilisation maintain Src family kinases plasma membrane localisation. *Nat Commun* 8: 114

Kosloff M, Elia N, Joel-Almagor T, Timberg R, Zars TD, Hyde DR, Minke B, Selinger Z (2003) Regulation of light-dependent Gqalpha translocation and morphological changes in fly photoreceptors. *EMBO J* 22: 459 – 468

Kozuka T, Chaya T, Tamalu F, Shimada M, Fujimaki-Aoba K, Kuwahara R, Watanabe SI, Furukawa T (2017) The TRPM1 channel is required for development of the rod ON bipolar cell-AII amacrine cell pathway in the retinal circuit. *J Neurosci* 37: 9889 – 9900

Liu J, Farmer JD Jr, Lane WS, Friedman J, Weissman I, Schreiber SL (1991) Calcineurin is a common target of cyclophilin-cyclosporin A and FKBP-FK506 complexes. *Cell* 66: 807 – 815

Luo DG, Xue T, Yau KW (2008) How vision begins: an odyssey. *Proc Natl Acad Sci USA* 105: 9855 – 9862

Majumder A, Pahlberg J, Boyd KK, Kerov V, Kolandaivelu S, Ramamurthy V, Sampath AP, Artemyev NO (2013) Transducin translocation contributes to rod survival and enhances synaptic transmission from rods to rod bipolar cells. *Proc Natl Acad Sci USA* 110: 12468 – 12473

Makino CL, Dodd RL, Chen J, Burns ME, Roca A, Simon MI, Baylor DA (2004) Recoverin regulates light-dependent phosphodiesterase activity in retinal rods. *J Gen Physiol* 123: 729 – 741

Marquioni-Ramella MD, Suburo AM (2015) Photo-damage, photo-protection and age-related macular degeneration. *Photochem Photobiol Sci* 14: 1560 – 1577

Matsuda T, Cepko CL (2004) Electroporation and RNA interference in the rodent retina *in vivo* and *in vitro*. *Proc Natl Acad Sci USA* 101: 16 – 22

Mattapallil MJ, Wawrousek EF, Chan CC, Zhao H, Roychoudhury J, Ferguson TA, Caspi RR (2012) The Rd8 mutation of the Crb1 gene is present in vendor lines of C57BL/6N mice and embryonic stem cells, and confounds ocular induced mutant phenotypes. *Invest Ophthalmol Vis Sci* 53: 2921 – 2927

McGourty CA, Akopian D, Walsh C, Gorur A, Werner A, Schekman R, Bautista D, Rape M (2016) Regulation of the CUL3 ubiquitin ligase by a calcium-dependent co-adaptor. *Cell* 167: 525 – 538 e514

Mears AJ, Kondo M, Swain PK, Takada Y, Bush RA, Saunders TL, Sieving PA, Swaroop A (2001) Nrl is required for rod photoreceptor development. *Nat Genet* 29: 447 – 452

Mendez A, Burns ME, Sokal I, Dizhoor AM, Baehr W, Palczewski K, Baylor DA, Chen J (2001) Role of guanylate cyclase-activating proteins (GCAPs) in setting the flash sensitivity of rod photoreceptors. *Proc Natl Acad Sci USA* 98: 9948 – 9953

Mitchell P, Liew G, Gopinath B, Wong TY (2018) Age-related macular degeneration. *Lancet* 392: 1147 – 1159

Moghe S, Jiang F, Miura Y, Cerny RL, Tsai MY, Furukawa M (2012) The CUL3-KLHL18 ligase regulates mitotic entry and ubiquitylates Aurora-A. *Biol Open* 1: 82 – 91

Muranishi Y, Terada K, Inoue T, Katoh K, Tsujii T, Sanuki R, Kurokawa D, Aizawa S, Tamaki Y, Furukawa T (2011) An essential role for RAX homeoprotein and NOTCH-HES signaling in Otx2 expression in embryonic retinal photoreceptor cell fate determination. *J Neurosci* 31: 16792 – 16807

Nakamura M, Yako T, Kuse Y, Inoue Y, Nishinaka A, Nakamura S, Shimazawa M, Hara H (2018) Exposure to excessive blue LED light damages retinal pigment epithelium and photoreceptors of pigmented mice. *Exp Eye Res* 177: 1 – 11

Nishida A, Furukawa A, Koike C, Tano Y, Aizawa S, Matsuo I, Furukawa T (2003) Otx2 homeobox gene controls retinal photoreceptor cell fate and pineal gland development. *Nat Neurosci* 6: 1255 – 1263

Okamoto S, Chaya T, Omori Y, Kuwahara R, Kubo S, Sakaguchi H, Furukawa T (2017) Ick ciliary kinase is essential for planar cell polarity formation in inner ear hair cells and hearing function. *J Neurosci* 37: 2073 – 2085

Omori Y, Chaya T, Katoh K, Kajimura N, Sato S, Muraoka K, Ueno S, Koyasu T, Kondo M, Furukawa T (2010) Negative regulation of ciliary length by ciliary male germ cell-associated kinase (Mak) is required for retinal photoreceptor survival. *Proc Natl Acad Sci USA* 107: 22671 – 22676

Omori Y, Katoh K, Sato S, Muranishi Y, Chaya T, Onishi A, Minami T, Fujikado T, Furukawa T (2011) Analysis of transcriptional regulatory pathways of photoreceptor genes by expression profiling of the Otx2-deficient retina. *PLoS One* 6: e19685

Omori Y, Kitamura T, Yoshida S, Kuwahara R, Chaya T, Irie S, Furukawa T (2015) Mef2d is essential for the maturation and integrity of retinal photoreceptor and bipolar cells. *Genes Cells* 20: 408 – 426

Omori Y, Kubo S, Kon T, Furuhashi M, Narita H, Kominami T, Ueno A, Tsutsumi R, Chaya T, Yamamoto H *et al* (2017) Samd7 is a cell type-specific PRC1 component essential for establishing retinal rod photoreceptor identity. *Proc Natl Acad Sci USA* 114: E8264 – E8273

Organisciak DT, Xie A, Wang HM, Jiang YL, Darrow RM, Donoso LA (1991) Adaptive changes in visual cell transduction protein levels: effect of light. *Exp Eye Res* 53: 773 – 779

Palczewski K, Subbaraya I, Gorczyca WA, Helekar BS, Ruiz CC, Ohguro H, Huang J, Zhao X, Crabb JW, Johnson RS *et al* (1994) Molecular cloning and characterization of retinal photoreceptor guanylyl cyclase-activating protein. *Neuron* 13: 395 – 404

Palczewski K, Sokal I, Baehr W (2004) Guanylate cyclase-activating proteins: structure, function, and diversity. *Biochem Biophys Res Commun* 322: 1123 – 1130

Pan ZQ, Kentsis A, Dias DC, Yamoah K, Wu K (2004) Nedd8 on cullin: building an expressway to protein destruction. *Oncogene* 23: 1985 – 1997

Parmeggiani F, Sato G, De Nadai K, Romano MR, Binotto A, Costagliola C (2011) Clinical and rehabilitative management of retinitis pigmentosa: up-to-date. *Curr Genomics* 12: 250 – 259

Paskowitz DM, LaVail MM, Duncan JL (2006) Light and inherited retinal degeneration. *Br J Ophthalmol* 90: 1060 – 1066

Peng YW, Zallocchi M, Wang WM, Delimont D, Cosgrove D (2011) Moderate light-induced degeneration of rod photoreceptors with delayed transducin translocation in shaker1 mice. *Invest Ophthalmol Vis Sci* 52: 6421 – 6427

Pettitt SJ, Liang Q, Rairdan XY, Moran JL, Prosser HM, Beier DR, Lloyd KC, Bradley A, Skarnes WC (2009) Agouti C57BL/6N embryonic stem cells for mouse genetic resources. *Nat Methods* 6: 493 – 495

Philp NJ, Chang W, Long K (1987) Light-stimulated protein movement in rod photoreceptor cells of the rat retina. *FEBS Lett* 225: 127 – 132

Rieke F, Baylor DA (1998) Origin of reproducibility in the responses of retinal rods to single photons. *Biophys J* 75: 1836 – 1857

Rosenzweig DH, Nair KS, Wei J, Wang Q, Garwin G, Saari JC, Chen CK, Smrcka AV, Swaroop A, Lem J *et al* (2007) Subunit dissociation and diffusion determine the subcellular localization of rod and cone transducins. *J Neurosci* 27: 5484 – 5494

Roska B, Sahel JA (2018) Restoring vision. *Nature* 557: 359 – 367

Sakai K, Miyazaki J (1997) A transgenic mouse line that retains Cre recombinase activity in mature oocytes irrespective of the cre transgene transmission. *Biochem Biophys Res Commun* 237: 318 – 324

Schick T, Ersoy L, Lechanteur YT, Saksens NT, Hoyng CB, den Hollander AI, Kirchhof B, Fauser S (2016) History of sunlight exposure is a risk factor for age-related macular degeneration. *Retina* 36: 787 – 790

Siddiqui-Jain A, Drygin D, Streiner N, Chua P, Pierre F, O'Brien SE, Bliesath J, Omori M, Huser N, Ho C *et al* (2010) CX-4945, an orally bioavailable selective inhibitor of protein kinase CK2, inhibits prosurvival and angiogenic signaling and exhibits antitumor efficacy. *Cancer Res* 70: 10288 – 10298

Sieving PA, Fowler ML, Bush RA, Machida S, Calvert PD, Green DG, Makino CL, McHenry CL (2001) Constitutive "light" adaptation in rods from G90D rhodopsin: a mechanism for human congenital nightblindness without rod cell loss. *J Neurosci* 21: 5449 – 5460

Sinha S, Majumder A, Belcastro M, Sokolov M, Artemyev NO (2013) Expression and subcellular distribution of UNC119a, a protein partner of transducin alpha subunit in rod photoreceptors. *Cell Signal* 25: 341 – 348

Slepak VZ, Hurley JB (2008) Mechanism of light-induced translocation of arrestin and transducin in photoreceptors: interaction-restricted diffusion. *IUBMB Life* 60: 2 – 9

Sokolov M, Lyubarsky AL, Strissel KJ, Savchenko AB, Govardovskii VI, Pugh EN Jr, Arshavsky VY (2002) Massive light-driven translocation of transducin between the two major compartments of rod cells: a novel mechanism of light adaptation. *Neuron* 34: 95 – 106

Soucy TA, Smith PG, Milhollen MA, Berger AJ, Gavin JM, Adhikari S, Brownell JE, Burke KE, Cardin DP, Critchley S *et al* (2009) An inhibitor of NEDD8-activating enzyme as a new approach to treat cancer. *Nature* 458: 732 – 736

Tian M, Wang W, Delimont D, Cheung L, Zallocchi M, Cosgrove D, Peng YW (2014) Photoreceptors in whirler mice show defective transducin translocation and are susceptible to short-term light/dark changes-induced degeneration. *Exp Eye Res* 118: 145 – 153

Trojan P, Rausch S, Giessl A, Klemm C, Krause E, Pulvermuller A, Wolfrum U (2008) Light-dependent CK2-mediated phosphorylation of centrins regulates complex formation with visual G-protein. *Biochim Biophys Acta* 1783: 1248 – 1260

Tsutsumi R, Chaya T, Furukawa T (2018) Enriched expression of the ciliopathy gene Ick in cell proliferating regions of adult mice. *Gene Expr Patterns* 29: 18 – 23

Ueno A, Omori Y, Sugita Y, Watanabe S, Chaya T, Kozuka T, Kon T, Yoshida S, Matsushita K, Kuwahara R *et al* (2018) Lrit1, a retinal transmembrane protein, regulates selective synapse formation in cone photoreceptor cells and visual acuity. *Cell Rep* 22: 3548 – 3561

Watanabe S, Sanuki R, Sugita Y, Imai W, Yamazaki R, Kozuka T, Ohsuga M, Furukawa T (2015) Prdm13 regulates subtype specification of retinal amacrine interneurons and modulates visual sensitivity. *J Neurosci* 35: 8004 – 8020

Wenzel A, Reme CE, Williams TP, Hafezi F, Grimm C (2001) The Rpe65 Leu450Met variation increases retinal resistance against light-induced degeneration by slowing rhodopsin regeneration. *J Neurosci* 21: 53 – 58

Whelan JP, McGinnis JF (1988) Light-dependent subcellular movement of photoreceptor proteins. *J Neurosci Res* 20: 263 – 270

Woodruff ML, Sampath AP, Matthews HR, Krasnoperova NV, Lem J, Fain GL (2002) Measurement of cytoplasmic calcium concentration in the rods of wild-type and transducin knock-out mice. *J Physiol* 542: 843 – 854

Wright KJ, Baye LM, Olivier-Mason A, Mukhopadhyay S, Sang L, Kwong M, Wang W, Pretorius PR, Sheffield VC, Sengupta P *et al* (2011) An ARL3-UNC119-RP2 GTPase cycle targets myristoylated NPHP3 to the primary cilium. *Genes Dev* 25: 2347 – 2360

Xu J, Dodd RL, Makino CL, Simon MI, Baylor DA, Chen J (1997) Prolonged photoresponses in transgenic mouse rods lacking arrestin. *Nature* 389: 505 – 509

Yau KW, Hardie RC (2009) Phototransduction motifs and variations. *Cell* 139: 246 – 264

Yoshida S, Mears AJ, Friedman JS, Carter T, He S, Oh E, Jing Y, Farjo R, Fleury G, Barlow C *et al* (2004) Expression profiling of the developing and mature $Nrl^{-/-}$ mouse retina: identification of retinal disease candidates and transcriptional regulatory targets of Nrl. *Hum Mol Genet* 13: 1487 – 1503

Zhang H, Li S, Doan T, Rieke F, Detwiler PB, Frederick JM, Baehr W (2007) Deletion of PrBP/delta impedes transport of GRK1 and PDE6 catalytic subunits to photoreceptor outer segments. *Proc Natl Acad Sci USA* 104: 8857 – 8862

Zhang H, Constantine R, Vorobiev S, Chen Y, Seetharaman J, Huang YJ, Xiao R, Montelione GT, Gerstner CD, Davis MW *et al* (2011) UNC119 is required for G protein trafficking in sensory neurons. *Nat Neurosci* 14: 874 – 880

